UCLA
COMPUTATIONAL AND APPLIED MATHEMATICS

Resistive Instabilities in Rapidly Rotating Fluids: Linear Theory of the Tearing Mode

Weijia Kuang
Paul H. Roberts

March 1990

CAM Report 90-07

Department of Mathematics
University of California, Los Angeles
Los Angeles, CA. 90024-1555

RESISTIVE INSTABILITIES IN RAPIDLY ROTATING FLUIDS: LINEAR THEORY OF THE TEARING MODE[1]

WEIJIA KUANG
Department of Mathematics, University of California, Los Angeles, California, CA 90024

PAUL H. ROBERTS
Center for Earth and Planetary Interiors, Institute of Geophysics and Planetary Physics, University of California, Los Angeles, California, CA 90024[2]

Received:

The linear stability of the sheet pinch is examined for a rapidly rotating fluid. The sheet pinch is a horizontal layer of uniform, incompressible, inviscid fluid of density ρ, electrical conductivity σ, magnetic permeability μ, confined between two perfectly conducting planes $z = 0, d$, where z is height. The prevailing magnetic field, $\mathbf{B}_0(z)$, is horizontal; at each height it is unidirectional, but that direction turns continuously (in one sense only) as z increases; the system is in magnetostatic equilibrium. The layer rotates about the vertical with an angular velocity, $\mathbf{\Omega}$, that is large: $\Omega \gg V_A/d$, where $V_A = B_0/\sqrt{(\mu\rho)}$ is the Alfvén velocity. The dimensionless number measuring σ is the Elsasser number $\Lambda = \sigma B_0^2/2\Omega\rho$.

The principal example studied here is force-free ($B_0 =$ constant);the direction of $\mathbf{B}_0$ rotates uniformly with height ($\nabla \times \mathbf{B}_0 = -q\mathbf{B}_0/d$, where q is a constant), turning through q radians between $z = 0$ and $z = d$.

The growth rate, s, of small perturbations of horizontal wave vector $\mathbf{k}$, is determined in a number of cases. It is found that instabilities do not occur if $\mathbf{B}_0$ makes less than one quarter turn between the boundaries. For $q > \frac{1}{2}\pi$, stability is lost when Λ exceeds a critical value, Λ_c, the instability being direct (i.e. the largest $\Re s$ is real, and this s is zero for $\Lambda = \Lambda_c$); as q increases, Λ_c decreases and s increases for any Λ. As Λ increases beyond Λ_c, s attains a maximum and then decreases monotonically to zero as $\Lambda \to \infty$.

The asymptotic form of the eigenmodes in the limit $\Lambda \to \infty$ is analysed in detail for general $\mathbf{B}_0$, especially their structure within the critical layers [of thickness $O(\Lambda^{-1/4}d)$] surrounding the critical levels, at which $\mathbf{k}$ is orthogonal to $\mathbf{B}_0$. The equilibrium is found to be more unstable when $\mathbf{J}_0 \times \mathbf{B}_0/\mathbf{J}_0.\mathbf{B}_0$ is antiparallel to $\mathbf{\Omega}$ than when it is parallel, $\mathbf{J}_0 = \nabla \times \mathbf{B}_0/\mu$ being the (horizontal) electric current density generating $\mathbf{B}_0$. It is shown that, provided this critical level is not asymptotically within one of the boundary layers [thickness $O(d\Lambda^{-1/2})$] at a wall, $s = O(\Lambda^{1/4}\tau_\eta^{-1})$, i.e. the instability develops more rapidly than the rate τ_η^{-1} ($= 1/\mu\sigma d^2$) at which $\mathbf{B}_0$ evolves through ohmic diffusion. Numerical evidence is presented, however, which indicates that, for the mode of maximum instability, the critical level moves into a boundary layer as $\Lambda \to \infty$.

KEY WORDS: resistive instability, tearing mode, sheet pinch, rotating magnetohydrodynamics.

---

[1]Contribution no.1 of the Center for Earth and Planetary Interiors, UCLA.

[2]Also at Department of Mathematics, University of California, Los Angeles, California, CA 90024.

owes its existence to the finiteness of σ; it would be absent in a perfectly conducting fluid. It is theoretically perhaps the most fascinating and most important of the resistive modes, the so-called "tearing mode" (Furth, Killeen and Rosenbluth, 1963). When $\sigma = \infty$, the topology of the magnetic field lines cannot be altered by fluid motions; they are "frozen" to the conductor (Alfvén's theorem). When σ is finite, the field lines can diffuse relative to the fluid and can reconnect in topologically new ways. If these result in highly bent field lines, there is a possibility that, by straightening up and carrying the (almost) frozen fluid with them as they do so, they can transform the magnetic energy of the equilibrium state into kinetic energy, i.e. create an instability that could not arise without the change in topology.

An instability of this type exists in the sheet pinch, the configuration studied in this paper. A uniform, electrically conducting, invisid, incompressible fluid occupies the "horizontal" layer $0 \leq z \leq d$, bounded by impermeable walls that are perfect electrical conductors. A horizontal field, $\mathbf{B}_0$, is present given by

$$\mathbf{B}_0 = B_{0x}(z)\hat{\mathbf{x}} + B_{0y}(z)\hat{\mathbf{y}}\,, \tag{1.1}$$

where $\hat{\mathbf{x}}$ and $\hat{\mathbf{y}}$ are the unit vectors in the coordinate directions. It is supposed that $\phi'(z)$ is nowhere zero in $[0, d]$, where

$$\phi(z) = \tan^{-1}(B_{0y}/B_{0x}) \tag{1.2}$$

is the angle between $\mathbf{B}_0$ and the x-axis. The field (1.1) then turns continuously about the "vertical" in one sense as z increases. The example of (1.1) on which we shall principally concentrate is the constant strength field,

$$\mathbf{B}_0 = B_0[\hat{\mathbf{x}}\,\cos\,qz/d + \hat{\mathbf{y}}\sin qz/d]\,, \tag{1.3}$$

for which B_0 and q are nonzero constants, and

$$\phi = qz/d\,.$$

Associated with $\mathbf{B}_0$ is a horizontal electric current, $\mathbf{J}_0$, given by

$$\mu\mathbf{J}_0 = \boldsymbol{\nabla}\times\mathbf{B}_0 = -DB_{0y}\,\hat{\mathbf{x}} + DB_{0x}\,\hat{\mathbf{y}}\,, \tag{1.4}$$

where$D = d/dz$. The Lorentz force, $\mathbf{J}_0 \times \mathbf{B}_0$, is balanced by the gradient of the pressure

$$P_0(z) = \text{constant} - \mathbf{B}_0^2/2\mu\,. \tag{1.5}$$

Hydrostatic equilibrium prevails; the velocity $\mathbf{V}$ of the fluid is everywhere zero. The field (1.3) is in fact "force-free"; since

$$\mathbf{J}_0 = (qB_0/\mu d)[\hat{\mathbf{x}}\cos\,qz/d + \hat{\mathbf{y}}\,\sin qz/d] = q\mathbf{B}_0/\mu d\,, \tag{1.6}$$

we have $\mathbf{J}_0 \times \mathbf{B}_0 = 0$.

The differences between the MHD of non-rotating and rapidly rotating fluids are so substantial as to invite us to re-examine the tearing mode when Coriolis forces are large and the layer is rotating about the vertical: $\mathbf{\Omega} = \Omega\hat{\mathbf{z}}$. Experts in MHD will correctly surmise that one of the more significant differences is that of timescales. In the "classical theory" (as we shall call the study of tearing in a non-rotating fluid) the two timescales of interest are the hydromagnetic (or Alfvén) timescale, τ_A, and the electromagnetic decay time, τ_η, where

$$\tau_A = \frac{H}{V_A}, \qquad \tau_\eta = \frac{H^2}{\eta}, \tag{1.7, 1.8}$$

where H is the horizontal scale of the instability (say the wavelength of the normal mode under study). The instability is studied in the conceptually simplest limit, $\Lambda \to \infty$, where Λ is the "Lundquist number," i.e. the ratio of timescales (1.8) and (1.7):

$$\Lambda = \frac{\tau_\eta}{\tau_A} = \frac{HV_A}{\eta}. \tag{1.9}$$

In a rapidly rotating fluid ($\Omega \gg V_A/H$) the role of the Alfvén wave is divided between the slow[3] and fast waves, with which are associated the timescales

$$\tau_s = \frac{2\Omega H^2}{V_A^2}, \qquad \tau_f = \frac{1}{2\Omega}, \tag{1.10, 1.11}$$

the former of which replaces τ_A as the important non-dissipative timescale. The limit of greatest interest is $\Lambda \to \infty$, where Λ is now the "Elsasser number", i.e. the ratio of the two timescales (1.8) and (1.10):

$$\Lambda = \frac{\tau_\eta}{\tau_s} = \frac{V_A^2}{2\Omega\eta} = \frac{\sigma B_0^2}{2\Omega\rho},$$

which is scale independent. Coriolis forces dominate inertial forces, and take over their role in the resistive modes of classical theory. The Elsasser number replaces the Lundquist number as the key non-dimensional parameter measuring electrical conductivity.

Unless Λ is large it is hard to visualize resistive modes in the terms we chose above, for when $\Lambda = O(1)$ the picture of field lines frozen to the conductor is seriously marred. Moreover, when $\Lambda = O(1)$, the growth rate of the instability (if any) can only be $O(\tau_\eta^{-1})$, the very same rate at which the field $\mathbf{B}_0$ is itself diffusively evolving. The development of $\mathbf{B}_0$ in time and its resistive instability would then, in general, be inextricably mixed, a serious theoretical handicap. The only exception to this statement would be if $\mathbf{B}_0$ had already completed its diffusive evolution to an electrodynamically steady state consistent with the boundary conditions applied. But, if that configuration were of minimum magnetic energy, no resistive instability could ensue; this is also true for such a $\mathbf{B}_0$ even when Λ is large (Barston, 1969).

It is now apparent that theoretically the clearest case arises when $\Lambda \gg 1$, and when τ_{instab} the timescale of the instability is short compared with τ_η, for it is only when $\tau_{\text{instab}} \ll$

[3]Because $\tau_s \ll \tau_\eta$, we earlier described τ_s as a "fast" timescale; since $\tau_f \ll \tau_s$, we here call τ_s "slow".

τ_η that one can ignore the diffusive evolution of $\mathbf{B}_0$ over the time during which it is destroyed by the instability. One may then, as we did in (1.1) or (1.2), select *any* $\mathbf{B}_0$ that is magnetostatic in the sense of ideal MHD ($\sigma = \infty$). One is left wondering however whether such a rapidly growing instability exists. It is clear that, to develop so quickly, the instability must operate in a region [which in the case of the field (1.1) is a horizontal "critical layer"] having a dimension, δ, small compared with H. The velocity, $V_{\rm drift}$, with which lines of force can drift relative to the conductor and reconnect is of order $V_{\rm drift} \approx \eta/\delta$ (e.g. see Roberts, 1967, p. 55). One can therefore expect the growth rate of the instability to be

$$\tau_{\rm instab} = \frac{d}{V_{\rm drift}} = \frac{d\delta}{\eta}\,. \tag{1.12}$$

The process is nevertheless slow compared with that of ideal wave propagation. Confining attention to the highly rotating case, $V_{\rm drift} \ll V_s$ $(= d/\tau_s)$, so that

$$\tau_s \ll \tau_{\rm instab} \ll \tau_\eta\,. \tag{1.13}$$

To determine δ, and to learn more about the structure of the critical layer of reconnection, consider a "normal mode" of instability, in which the perturbation field,

$$\mathbf{b} = \mathbf{B} - \mathbf{B}_0\,, \tag{1.14}$$

is proportional to

$$\exp[i(k_x x + k_y y) + st]\,, \tag{1.15}$$

where

$$k_x = k\,\cos\,\theta, \qquad k_y = k\,\sin\,\theta\,, \tag{1.16}$$

are the horizontal wavenumbers of the mode and s is its growth rate. The phase fronts make an angle of $\theta - \phi$ with $\mathbf{B}_0$ so that, at a "critical level", at which $\theta = \phi \pm \frac{1}{2}\pi$, the slow wave propagates in the direction perpendicular to that in which the instability moves. Within a critical layer of width, δ, surrounding the critical level, the effective strength of $\mathbf{B}_0$ is therefore effectively reduced by a factor of order δ/H, i.e. to $\mathbf{B}_0\delta/H$. The fluid motions $\mathbf{v}$ (required in the critical layer, to balance by electromagnetic induction the rate, $\eta\mathbf{b}/\delta^2$, at which field diffuses and reconnects) is therefore correspondingly larger. Thus $\eta\mathbf{b}/\delta^2$ is not of order $\mathbf{v}B_0/d$ but is $O(\mathbf{v}B_0\delta/Hd)$, which implies that $\mathbf{v} = O(\eta Hd\mathbf{b}/B_0\delta^3)$. This is true also for the classical tearing mode. The dynamical balances in the non-rotating and highly rotating layers are, however, very different. In the former, Lorentz force is balanced by inertial forces; in the latter, it is balanced by Coriolis force. Because of the effective reduction in $\mathbf{B}_0$ in the critical layer, the Lorentz force is not of order $B_0\mathbf{j} = O(B_0\mathbf{b}/\mu d)$, but is of order $B_0\mathbf{b}\delta/\mu Hd$. When this is set against a Coriolis force that is $O(2\Omega\rho\mathbf{v})$, we obtain $\mathbf{b} = O(2\Omega\mu\rho Hd\mathbf{v}/B_0\delta)$. Combining this with our earlier estimate, $\mathbf{v} = O(\eta Hd\mathbf{b}/B_0\delta^3)$, we see that

$$\delta = O(H^{1/2}d^{1/2}\Lambda^{-1/4})\,, \qquad \tau_{\rm instab} = O\left[(d/H)^{3/2}\ \tau_s^{1/4}\tau_\eta^{3/4}\right]\,. \tag{1.17, 1.18}$$

The latter follows from (1.12); obviously (1.13) is satisfied.

2. Basic Equations and Boundary Conditions

We study the motion of a uniform, invisid, incompressible fluid in the so-called "magnetostrophic approximation", in which inertial forces are neglected:

$$2\boldsymbol{\Omega}\times\mathbf{V} = -\boldsymbol{\nabla}P + \frac{1}{\rho}\,\mathbf{J}\times\mathbf{B}\,, \tag{2.1}$$

$$\frac{\partial\mathbf{B}}{\partial t} = \boldsymbol{\nabla}\times(\mathbf{V}\times\mathbf{B}) + \eta\nabla^2\mathbf{B}\,, \tag{2.2}$$

$$\boldsymbol{\nabla}\cdot\mathbf{V} = 0\,, \qquad \boldsymbol{\nabla}\cdot\mathbf{B} = 0\,. \tag{2.3, 2.4}$$

Here P is the reduced pressure (pressure divided by the constant density ρ and including centrifugal forces), and $\mathbf{J} = \mu^{-1}\boldsymbol{\nabla}\times\mathbf{B}$ is the electric current density.

The field (1.1) satisfies the hydrostatic form of (2.1):

$$\mathbf{V}_0 \equiv 0\,, \qquad 0 = -\boldsymbol{\nabla}P_0 + \frac{1}{\rho}\,\mathbf{J}_0\times\mathbf{B}_0\,, \tag{2.5}$$

but not (2.2). As explained in Section 1 we suppose that $\Lambda \gg 1$ so that the diffusive evolution of $\mathbf{B}_0$ is too slow to be a factor. We study the linear stability of field (1.1) by writing

$$\mathbf{B} = \mathbf{B}_0 + \mathbf{b}\,, \quad \mathbf{J} = \mathbf{J}_0 + \mathbf{j}\,, \quad \mathbf{V} = \mathbf{V}_0 + \mathbf{v}\,, \quad P = P_0 + p\,, \tag{2.6}$$

substituting into (2.1)–(2.4), simplifying with the help of (2.5), and linearizing in the usual way. We obtain

$$\hat{\mathbf{z}}\times\mathbf{v} = -\boldsymbol{\nabla}p + \mathbf{B}_0\cdot\boldsymbol{\nabla}\mathbf{b} + \mathbf{b}\cdot\boldsymbol{\nabla}\mathbf{B}_0\,, \tag{2.7}$$

$$\frac{\partial\mathbf{b}}{\partial t} = \frac{1}{\Lambda}\,\nabla^2\mathbf{b} + \mathbf{B}_0\cdot\boldsymbol{\nabla}\mathbf{v} - \mathbf{v}\cdot\boldsymbol{\nabla}\mathbf{B}_0\,, \tag{2.8}$$

$$\boldsymbol{\nabla}\cdot\mathbf{v} = 0\,, \qquad \boldsymbol{\nabla}\cdot\mathbf{b} = 0\,. \tag{2.9}$$

We have here absorbed the perturbed magnetic pressure $\mathbf{B}_0\cdot\mathbf{b}/\mu$ into p, and have made the equation dimensionless by the transformation

$$\begin{gathered}\mathbf{x}\to d\mathbf{x}\,, \quad t\to\tau_s t\,, \quad \mathbf{v}\to(d/\tau_s)\,\mathbf{v}\,,\\ \mathbf{B}\to\mathcal{B}\mathbf{B}\,, \quad \mathbf{b}\to\mathcal{B}\mathbf{b}\,, \quad p\to(2\Omega d^2/\tau_s)p\,,\end{gathered} \tag{2.10}$$

where $\mathcal{B}$ is a typical scale for $\mathbf{B}_0$ and from now onward

$$\tau_s = \frac{2\Omega\mu\rho d^2}{\mathcal{B}^2}\,, \qquad \tau_\eta = \frac{d^2}{\eta}\,, \qquad \Lambda = \frac{\tau_\eta}{\tau_s}\,. \tag{2.11}$$

After eliminating p, we find that (2.7)–(2.9) require that

$$D v_z = \hat{\mathbf{z}}\cdot D\mathbf{B}_0\times\boldsymbol{\nabla}b_z - (\mathbf{B}_0\cdot\boldsymbol{\nabla})j_z\,, \tag{2.12}$$

$$D\omega_z = (\mathbf{B}_0 \cdot \boldsymbol{\nabla})\nabla^2 b_z - (D^2\mathbf{B}_0)\cdot\boldsymbol{\nabla} b_z\,, \tag{2.13}$$

$$\left(\frac{\partial}{\partial t} - \frac{1}{\Lambda}\nabla^2\right) b_z = (\mathbf{B}_0 \cdot \boldsymbol{\nabla}) v_z\,, \tag{2.14}$$

$$\left(\frac{\partial}{\partial t} - \frac{1}{\Lambda}\nabla^2\right) j_z = (\mathbf{B}_0 \cdot \boldsymbol{\nabla})\omega_z + \hat{\mathbf{z}}\cdot D\mathbf{B}_0 \times \boldsymbol{\nabla} v_z\,, \tag{2.15}$$

where $\boldsymbol{\omega}$ $(= \boldsymbol{\nabla}\times\mathbf{v})$ and $\mathbf{j}$ $(= \boldsymbol{\nabla}\times\mathbf{b})$ are the dimensionless vorticity and perturbed current density; $D = d/dz$.

We seek normal mode solution of (2.12)–(2.15) of the form (1.15) so that

$$Dv_z = -i(Fj_z + \bar{F}b_z)\,, \tag{2.16}$$

$$D\omega_z = i[F(D^2 - k^2)b_z - (D^2F)b_z]\,, \tag{2.17}$$

$$[\Lambda^{-1}(D^2 - k^2) - s]b_z = -iFv_z\,, \tag{2.18}$$

$$[\Lambda^{-1}(D^2 - k^2) - s]j_z = -i(F\omega_z - \bar{F}v_z)\,, \tag{2.19}$$

where

$$F = k_x B_{0x} + k_y B_{0y}, \qquad \bar{F} = D(k_x B_{0y} - k_y B_{0x})\,. \tag{2.20}$$

We must solve the sixth order system (2.16)–(2.19) subject to three conditions at each of $z = 0$ and $z = 1$. We shall suppose that these boundaries are impermeable, perfectly conducting walls, so that

$$v_z = b_z = Dj_z = 0\,, \qquad z = 0, 1\,. \tag{2.21}$$

3. The Limit $\Lambda \to \infty$. Critical Layer Analysis

If we formally set $\Lambda = \infty$ in (2.16)–(2.20), that sixth order system system collapses to the second order problem of finding s_0^2 such that

$$s_0^2\, D\left[\frac{1}{F^2}\, D\left(\frac{b_z^{(0)}}{F}\right)\right] + F(D^2 - k^2)b_z^{(0)} - (D^2F)b_z^{(0)} = 0\,, \tag{3.1}$$

together with

$$b_z^{(0)}(0) = b_z^{(0)}(1) = 0\,, \tag{3.2}$$

possesses a nontrivial solution. Here s_0 is the growth rate to leading order in Λ.

By multiplying (3.1) by $b_z^{(0)*}/F$, integrating by parts and applying (3.2), it is easily seen that, if F has no zero in $[0, 1]$, i.e. if there is no critical level, then

$$\int_0^1 \left[\left(F^2 + \frac{s_0^2}{F^2}\right)\left|D\left(\frac{b_z^{(0)}}{F}\right)\right|^2 + k^2|b_z^{(0)}|^2\right]\, dz = 0\,. \tag{3.3}$$

It follows that s_0^2 is real and negative, i.e. there is no instability. Supposing $s_0 \neq 0$, it is conceivable that this oscillation, which is purely sinusoidal for $\Lambda = \infty$, might be growing

slowly for $\Lambda \gg 1$, i.e. s might have a positive real part of order Λ^{-1} for $\Lambda \to \infty$. We have been unable to establish this; nor have we been able to show that the principle of the exchange of stabilities holds for the system (2.16)–(2.20), although our numerical work (see Section 5) in no case located a growing overstable mode. From now on we shall assume that s_0 is zero, so that

$$F(D^2 - k^2)b_z^{(0)} - (D^2 F)b_z^{(0)} = 0\,. \tag{3.4}$$

More precisely, we suppose that $s < O(1)$, so that it does not appear in the leading order equation (3.4). We shall regard (3.4) as governing the "outer solution" away from the boundaries at $z = 0$ and $z = 1$, and away also from critical levels.

There may be more than one critical level, but for simplicity we shall here suppose that there is only one, and that it is situated at $z = z_c$, where $0 < z_c < 1$. We then have

$$F(z_c) = 0\,, \tag{3.5}$$

and, in a sufficiently small neighborhood of $z = z_c$,

$$F(z) = F_c'(z - z_c)\,, \tag{3.6}$$

where $F_c' \equiv F'(z_c) \neq 0$. In this neighborhood, the solution of (3.4) we require may be written as a linear combination of the two solutions

$$b_{z1}^{(0)} = 1, \qquad b_{z2}^{(0)} = z - z_c\,, \tag{3.7}$$

i.e. $b_z^{(0)}$ is proportional to $1 + A(z - z_c)$. As for the classical tearing mode, A changes discontinuously at $z = z_c$, i.e.

$$b_z^{(0)} = \begin{cases} 1 + A_+(z - z_c)\,, & z \to z_c+\,, \\ 1 + A_-(z - z_c)\,, & z \to z_c-\,. \end{cases} \tag{3.8}$$

It is to this discontinuity that tearing modes owe their instability.

To determine the discontinuity $A_+ - A_-$ in Db_z at $z = z_c$, or more precisely to find

$$\Delta \equiv \left[\frac{Db_z^{(0)}}{b_z^{(0)}}\right]_{z_c-}^{z_c+}\,, \tag{3.9}$$

it is necessary to analyse the structure of the critical layer. This will occupy the remainder of this Section.

It follows from (2.16)–(2.19) by elimination that

$$\begin{aligned} D\left[\left[\frac{1}{F}\left\{\frac{1}{\Lambda}(D^2 - k^2) - s\right\}\frac{1}{F}D\left[\frac{1}{F}\left\{\frac{1}{\Lambda}(D^2 - k^2) - s\right\}b_z\right]\right]\right] \\ + \frac{1}{\Lambda}D\left[\frac{1}{F}\left\{2D\left(\frac{\bar{F}}{F}\right)Db_z + D^2\left(\frac{\bar{F}}{F}\right)b_z\right\}\right] + F(D^2 - k^2)b_z - (D^2 F)b_z = 0. \end{aligned} \tag{3.10}$$

In the critical layer we may replace F by (3.6) and use the stretched coordinate ζ in place of z, where

$$z = z_c + \zeta\delta\,. \tag{3.11}$$

Understanding D now to be $d/d\zeta$, we find that, in the leading order,

$$D\left[\!\!\left[\frac{1}{\zeta^2}D\left\{\zeta^2 D\left(\frac{1}{\zeta^2}D\right)^2\zeta^2\right\} + \left(\zeta^2 + \frac{2\alpha}{\zeta^2}\right)\right]\!\!\right] D\left(\frac{b_z}{\zeta}\right)$$
$$= pD\left\{\frac{1}{\zeta^2}\left(2D^2 - p\right)\right\} D\left(\frac{b_z}{\zeta}\right)\,, \tag{3.12}$$

where

$$p = s\Lambda\delta^2 \tag{3.13}$$

is the scaled growth rate; $p \ll 1$, by the arguments of Section 1. The boundary layer thickness is

$$\delta = \frac{1}{|F_c'|^{1/2}\Lambda^{1/4}}\,, \tag{3.14}$$

and

$$\alpha = -\frac{\bar{F}_c}{F_c'} = \left(\frac{\hat{\mathbf{z}}\cdot\mathbf{J}_0\times\mathbf{B}_0}{\mathbf{J}_0\cdot\mathbf{B}_0}\right)_{z_c}\,. \tag{3.15}$$

In our model (1.3), $\alpha \equiv 0$, and in what follows we shall suppose not only that $p \ll 1$ but also that $\alpha \ll 1$. We shall therefore replace (3.12) by

$$D\left[\!\!\left[\frac{1}{\zeta^2}D\left\{\zeta^2 D\left(\frac{1}{\zeta^2}D\right)^2\zeta^2\right\} + \zeta^2\right]\!\!\right] D\left(\frac{b_z}{\zeta}\right)$$
$$= 2pD\left[\frac{1}{\zeta^2}D^3\left(\frac{b_z}{\zeta}\right)\right] - 2\alpha D\left[\frac{1}{\zeta^2}D\left(\frac{b_z}{\zeta}\right)\right]\,, \tag{3.16}$$

and regard the right-hand side as a perturbation.

The homogeneous equation,

$$\left[D\left(\frac{1}{\zeta^2}D\right)(\zeta^2 D)\left(\frac{1}{\zeta^2}D\right) + \zeta^2\right]\left(\frac{1}{\zeta}D^2 w\right) = 0\,, \tag{3.17}$$

obtained by setting the right-hand side of (3.16) zero, admits the solutions

$$w_1 = 1\,, \qquad w_2 = \zeta\,. \tag{3.18}$$

In fact w_2 is also an exact solution of (3.16) and (3.12). It corresponds to the solution $b_{z2}^{(0)}$ given in (3.7), and demonstrates that this solution passes through the critical layer unaffected, i.e. it is only the difference, Δ, between A_+ and A_- that is significant in (3.8). We may therefore take $A_+ = -A_-(= A$, say) without loss of generality, so that in the critical layer

$$b_z(-\zeta) \equiv b_z(\zeta)\,, \tag{3.19}$$

and

$$b_z \sim A|\zeta|\,, \qquad \zeta \to \pm\infty\,, \tag{3.20}$$

where $A = \frac{1}{2}\,\Delta\,\delta$; see (3.8), (3.9) and (3.11). The objective is to determine $A(p,\alpha)$.

Since we are interested only in even b_z, we need consider only two of the remaining four solutions of (3.17), namely

$$w_3 = \sum_{n=0}^{\infty} \frac{(-1)^n(\zeta/2^{3/2})^{8n}}{n!\,\Gamma\left(n+\frac{1}{4}\right)\Gamma\left(n+\frac{3}{8}\right)\Gamma\left(n+\frac{5}{8}\right)\left(n-\frac{1}{8}\right)} \tag{3.21}$$

$$w_4 = \sum_{n=0}^{\infty} \frac{(-1)^n(\zeta/2^{3/2})^{8n+6}}{n!\,\Gamma\left(n+\frac{7}{4}\right)\Gamma\left(n+\frac{9}{8}\right)\Gamma\left(n+\frac{11}{8}\right)\left(n+\frac{5}{8}\right)}\,. \tag{3.22}$$

It may be noted that these are entire functions, and that the series converge for all complex ζ. Also, if k is an integer,

$$w_3(\zeta e^{k\pi i/4}) \equiv w_3(\zeta)\,, \qquad w_4(\zeta e^{k\pi i/4}) \equiv e^{3k\pi i/4} w_4(\zeta)\,. \tag{3.23}$$

They therefore satisfy (3.19); $k = 4$. We shall therefore confine attention to the sector

$$|\arg\zeta| < \tfrac{1}{8}\,\pi\,. \tag{3.24}$$

We may write w_3 and w_4 as contour integrals:

$$w_3 = \frac{1}{2\pi i}\int_{C_3} \frac{(\zeta/2^{3/2})^{8s}\pi\,\mathrm{cosec}\pi s\;ds}{\Gamma(s+1)\Gamma\left(s+\frac{1}{4}\right)\Gamma\left(s+\frac{3}{8}\right)\Gamma\left(s+\frac{5}{8}\right)\left(s-\frac{1}{8}\right)}\,, \tag{3.25}$$

$$w_4 = \frac{1}{2\pi i}\int_{C_4} \frac{(\zeta/2^{3/2})^{8s+6}\pi\,\mathrm{cosec}\pi s\;ds}{\Gamma(s+1)\Gamma\left(s+\frac{7}{4}\right)\Gamma\left(s+\frac{9}{8}\right)\Gamma\left(s+\frac{11}{8}\right)\left(s+\frac{5}{8}\right)}\,. \tag{3.26}$$

Here C_4 passes from $s = \infty + 0i$ to $s = \infty - 0i$, to the left of $s = 0$ but to the right of $s = -\frac{5}{8}$; C_3 is similar but is distorted to avoid surrounding $s = \frac{1}{8}$. See Figures 1. Both contours surround the poles of the integrands at $s = n$, where n is a non-negative integer; because of the $\Gamma(s+1)$ factors, the negative integers are not poles of the integrands. Both integrands have saddle points near

$$s = \tfrac{1}{8}\,\zeta^2 e^{\pm i\pi/4}\,, \tag{3.27}$$

and, by standard applications of the method of steepest descent, it is found that, to leading order as $\zeta \to \infty$ in sector (3.24),

$$w_3 \sim \frac{1}{(2\pi)^{3/2}}\left(\frac{8}{\zeta^2}\right)^{3/4} e^{\zeta^2/2\sqrt{2}}\cos\left(\frac{\zeta^2}{2\sqrt{2}} - \frac{3\pi}{16}\right)\,, \tag{3.28}$$

$$w_4 \sim \frac{1}{(2\pi)^{3/2}}\left(\frac{8}{\zeta^2}\right)^{3/4} e^{\zeta^2/2\sqrt{2}}\cos\left(\frac{\zeta^2}{2\sqrt{2}} - \frac{15\pi}{16}\right)\,. \tag{3.29}$$

We now return to the inhomogeneous equation (3.16), and write its solution as

$$b_z = 1 + pb_{zp} - \alpha b_{z\alpha}\,, \tag{3.30}$$

where, to leading order in p and α,

$$\left[D\left(\frac{1}{\zeta^2}\,D\right)(\zeta^2 D)\left(\frac{1}{\zeta^2}\,D\right) + \zeta^2\right]\frac{1}{\zeta}\,D^2 b_{zp} = \frac{72}{\zeta^7}\,, \tag{3.31}$$

$$\left[D\left(\frac{1}{\zeta^2}\,D\right)(\zeta^2 D)\left(\frac{1}{\zeta^2}\,D\right) + \zeta^2\right]\frac{1}{\zeta}\,D^2 b_{z\alpha} = \frac{8}{\zeta^5}\,. \tag{3.32}$$

The right-hand sides are obtained by setting $b_z = 1$, the dominant part of (3.30), into the right-hand side of (3.16). Particular solutions satisfying (3.19) are

$$b^P_{zp} = c_p \sum_{n=0}^{\infty} \frac{(-1)^n(\zeta/2^{3/2})^{8n+2}}{\Gamma\left(n+\frac{1}{2}\right)\Gamma\left(n+\frac{5}{8}\right)\Gamma\left(n+\frac{7}{8}\right)\Gamma\left(n+\frac{5}{4}\right)\left(n+\frac{1}{8}\right)}\,, \tag{3.33}$$

$$b^P_{z\alpha} = c_\alpha \sum_{n=0}^{\infty} \frac{(-1)^n(\zeta/2^{3/2})^{8n+4}}{\Gamma\left(n+\frac{3}{4}\right)\Gamma\left(n+\frac{7}{8}\right)\Gamma\left(n+\frac{9}{8}\right)\Gamma\left(n+\frac{3}{2}\right)\left(n+\frac{3}{8}\right)}\,. \tag{3.34}$$

where

$$c_p = \frac{\sqrt{\pi}}{8}\,\Gamma\left(\frac{1}{4}\right)\Gamma\left(\frac{5}{8}\right)\Gamma\left(\frac{7}{8}\right)\,, \tag{3.35}$$

$$c_\alpha = \frac{\pi^{3/2}}{8\sin(\pi/8)}\,\Gamma\left(\frac{3}{4}\right)\,. \tag{3.36}$$

After forming integral representations similar to (3.25) and (3.26) we find from a steepest descent analysis of the saddle points near (3.27) that, as $\zeta \to \infty$ in sector (3.24),

$$b^P_{zp} \sim \frac{c_p}{(2\pi)^{3/2}}\left(\frac{8}{\zeta^2}\right)^{3/4} e^{\zeta^2/2\sqrt{2}}\cos\left(\frac{\zeta^2}{2\sqrt{2}} - \frac{7\pi}{16}\right)\,, \tag{3.37}$$

$$b^P_{z\alpha} \sim \frac{c_\alpha}{(2\pi)^{3/2}}\left(\frac{8}{\zeta^2}\right)^{3/4} e^{\zeta^2/2\sqrt{2}}\cos\left(\frac{\zeta^2}{2\sqrt{2}} - \frac{11\pi}{16}\right)\,. \tag{3.38}$$

Evidently the particular integrals (3.33) and (3.34) do not match to (3.20), but by adding appropriate multiples of w_3 and w_4 we can eliminate the exponentially increasing terms (3.37) and (3.38). We therefore replace b^P_{zp} and $b^P_{z\alpha}$ by

$$b_{zp} = b^P_{zp} - 2^{1/2}c_p w_3 - c_p w_4\,, \tag{3.39}$$

$$b_{z\alpha} = b^P_{z\alpha} - c_\alpha w_3 - 2^{1/2}c_\alpha w_4\,. \tag{3.40}$$

Returning to the series representation (3.21), (3.22), (3.33) and (3.34) we find the more convenient forms

$$b_{zp} = -\frac{c_p}{\sqrt{2}}\,(W + W^*)\,, \tag{3.41}$$

$$b_{z\alpha} = -\frac{c_\alpha}{\sqrt{2}}\,[e^{3i\pi/4}W + e^{-3i\pi/4}W^*]\,, \tag{3.42}$$

where

$$W = \sum_{m=0}^{\infty} \frac{(-1)^m (\zeta^2 e^{-\pi i/4}/8)^m}{\Gamma\left(\frac{m}{4}+\frac{1}{4}\right)\Gamma\left(\frac{m}{4}+\frac{3}{8}\right)\Gamma\left(\frac{m}{4}+\frac{5}{8}\right)\Gamma\left(\frac{m}{4}+1\right)\left(\frac{m}{4}-\frac{1}{8}\right)}\,. \tag{3.43}$$

It may be shown (see Appendix) that

$$W \sim \frac{8(2\pi)^{1/2} e^{7\pi i/8}}{\Gamma\left(\frac{1}{8}\right)\Gamma\left(\frac{3}{8}\right)\Gamma\left(\frac{3}{4}\right)}\,\zeta\,, \qquad \zeta \to \infty\,. \tag{3.44}$$

It follows from (3.20), (3.30), (3.41) and (3.42) that

$$A = A_p p + A'_\alpha \alpha\,, \tag{3.45}$$

where

$$A_p = 2\pi^2\,\frac{\Gamma\left(\frac{1}{4}\right)\Gamma\left(\frac{7}{8}\right)}{\Gamma\left(\frac{3}{4}\right)\Gamma\left(\frac{1}{8}\right)\left[\Gamma\left(\frac{3}{8}\right)\right]^2} \doteq 1.5032\ldots, \tag{3.46}$$

$$A'_\alpha = \frac{2\pi^2}{\Gamma\left(\frac{1}{8}\right)\Gamma\left(\frac{3}{8}\right)} \doteq 1.1053\ldots \tag{3.47}$$

These results, which are valid only for $|p| \ll 1$ and $|\alpha| \ll 1$, were verified numerically by using a specially constructed program for critical layer integration (see Appendix B). It was found that, for larger values of α, (3.45) is replaced by

$$A = A_p(\alpha) p + A_\alpha(\alpha)\,, \tag{3.48}$$

where $A_p(\alpha)$ and $A_\alpha(\alpha)$ took the values shown in Table 1 for $-10 \le \alpha \le 10$. The numerical value of $A'_\alpha(0)$ was 1.1056, which should be compared with (3.47).

Unlike classical tearing, for which the growth rate for given $\mathbf{k}$ is determined when $\Lambda \gg 1$ not by B_{0x} and B_{0y} individually but only in the combination, F, the rate of tearing in a highly rotating fluid is affected by the magnetic helicity at each critical level, as measured by α. Let us compare tearing for $k_x = k_y$ in the field (1.3) for $q = \frac{3}{2}\,\pi$, i.e.

$$\mathbf{B}_0^{(1)} = \hat{\mathbf{x}} \cos\frac{3}{2}\,\pi z + \hat{\mathbf{y}}\,\sin\frac{3}{2}\,\pi z\,, \tag{3.49}$$

with tearing in the field

$$\mathbf{B}_0^{(2)} = \hat{\mathbf{x}}\left(\cos\frac{3}{2}\,\pi z + \frac{3\alpha}{2\sqrt{2}}\cos\pi z\right) + \hat{\mathbf{y}}\left(\sin\frac{3}{2}\,\pi z - \frac{3\alpha}{2\sqrt{2}}\,\cos\pi z\right)\,. \tag{3.50}$$

Since F is the same for each, marginal stability is decided by the same value of $A = \frac{1}{2}\,\Delta\delta$ at the single critical point $z_c = \frac{1}{2}$. By (3.15) we have $\alpha^{(1)} = 0$, $\alpha^{(2)} = \alpha$. For $\alpha > 0$ we see from (3.45) or (3.48) that p is larger in case (3.49) than in case (3.50), as therefore is the growth rate, s, of the instability.

4. The Limit $\Lambda = \infty$. Examples

The principal form for $\mathbf{B}_0$ studied in this paper is (1.3) for which [see also (1.16)]

$$F = k\cos(\theta - qz)\,, \qquad \bar{F} = -qF\,. \tag{4.1, 4.2}$$

Clearly F is unchanged under the transformation

$$z \to 1 - z\,, \qquad \theta \to q - \theta\,, \tag{4.3S}$$

while its sign is reversed if

$$z \to 1 - z\,, \qquad \theta \to \pi + q - \theta\,. \tag{4.3A}$$

In either case (3.10) is unaltered. At first sight it might seem that, once one has obtained a solution for one choice of $\mathbf{k}$, we could obtain a second by one of the transformations (4.3S) or (4.3A), and that in this new solution

$$b_z(z) \to b_z(1 - z)\,. \tag{4.4}$$

This hope is, however, frustrated by the boundary conditions on b_z implied by (2.21). This may also be seen directly from (2.16)–(2.19): the symmetries

$$b_z \to b_z\,, \quad v_z \to v_z\,, \quad \omega_z \to -\omega_z\,, \quad j_z \to -j_z\,, \tag{4.5S}$$

and

$$b_z \to -b_z\,, \quad v_z \to -v_z\,, \quad \omega_z \to \omega_z\,, \quad j_z \to j_z\,, \tag{4.5A}$$

expected from (4.3S) and (4.3A) are destroyed by the $\bar{F}$ terms in (2.16) and (2.19). There are however exceptional choices of $\mathbf{k}$, namely

$$\theta = \frac{1}{2}\,q + m\pi\,, \qquad \theta = \frac{1}{2}\,q + \left(m + \frac{1}{2}\right)\pi\,, \tag{4.6S}$$

for which F is symmetric or antisymmetric when m is an integer. In these cases solutions satisfying symmetries (4.5S) or (4.5A) exist. Moreover, even for general q, the effectiveness of the $\bar{F}$ terms in (2.16) and (2.19) diminishes continually as Λ increases and, to leading order in the limit $\Lambda \to \infty$, (4.3S) are (4.3A) do imply new solutions obtained respectively from (4.5S) and (4.5A).

According to (4.1), if $n\pi < q < (n+1)\pi$ where $n(\geq 0)$ is an integer, there may be either n or $n+1$ critical levels in $(0,1)$, depending on the choice of θ. The existence of a critical level does not guarantee that an instability exists in the limit $\Lambda \to \infty$, as the case $n = 0$ described below will show. In general the greater the number of critical levels, the more magnetic energy will become available to an instability, and the greater the growth rate, s.

From now onwards, suppose that

$$0 < \ q \ \leq \ 2\pi\,. \tag{4.7}$$

There is only one critical level (at $z = z_c$, say) if either

(i) $0 < q \leq \pi$, or

(ii) $\pi < q < 2\pi$ and $1 - \pi/q < z_c < \pi/q$.

There are two critical levels (at $z = z_{c1}, z_{c2}$, say) if

(iii) $\pi < q \leq 2\pi$, and $0 < z_{c1} < 1 - \pi/q$;

then $z_{c2} = z_{c1} + \pi/q$, so that $\pi/q < z_{c2} < 1$.

In all these cases

$$\alpha = 0\,, \qquad |F_0'| = kq\,. \tag{4.8, 4.9}$$

We shall now find, in the limit $\Lambda \to \infty$, the unstable modes in cases (i)–(iii). Away from critical points and boundary layers, the solution to leading order obeys (3.4), which reduces for field (1.3) to

$$D^2 b_z^{(0)} = (k^2 - q^2) b_z^{(0)}\,. \tag{4.10}$$

First consider cases (i) and (ii).

(A) Suppose that $k > q$ and let $\beta = (k^2 - q^2)^{1/2}$. Then, by (3.2),

$$b_z^{(0)} = \begin{cases} \sinh\ \beta z / \sinh\ \beta z_c\,, & \text{if } z \leq z_c\,; \\ \sinh\ \beta(1-z) / \sinh\ \beta(1-z_c)\,, & \text{if } z \geq z_c\,, \end{cases} \tag{4.11}$$

so that

$$\Delta \equiv \left[\frac{D b_z^{(0)}}{b_z^{(0)}}\right]_c = -\beta[\coth\ \beta z_c + \coth\ \beta(1-z_c)]\,; \tag{4.12}$$

see (3.9). But according to the critical layer analysis of Section 3, we must have

$$\Delta > 0\,, \quad \text{for instability}\,. \tag{4.13}$$

It follows that disturbances of short wavelength are always stable.

(B) Suppose next that $k < q$ and let $\gamma = (q^2 - k^2)^{1/2}$. In place of (4.11) and (4.12) we have

$$b_z^{(0)} = \begin{cases} \sin\ \gamma z / \sin\ \gamma z_c\,, & \text{if } z \leq z_c\,; \\ \sin\ \gamma(1-z) / \sin\ \gamma(1-z_c)\,, & \text{if } z \geq z_c\,, \end{cases} \tag{4.14}$$

$$\Delta = -\frac{\gamma \sin\gamma}{\sin\ \gamma z_c\ \sin\ \gamma(1-z_c)}\,. \tag{4.15}$$

Since $\gamma < q$, we have

$$0 < \gamma z_c < q z_c < \pi\,, \qquad 0 < \gamma(1-z_c) < q(1-z_c) < \pi\,. \tag{4.16}$$

The denominator of (4.15) is therefore necessarily positive. Thus instability can arise only if $\pi < \gamma < 2\pi$. Since $\gamma < q$, this means that an instability cannot occur in case (i), but may arise in case (ii).

To find the growth rate of the instability in case (ii), it is merely a matter of equating Δ is (4.15) to the expression $2A/\delta$ implied by (3.20), A being given by (3.45), (3.46) and (4.8). We obtain, using also (3.14) and (4.9),

$$p \sim \frac{\gamma|\sin\gamma|}{3.0065(kq)^{1/2} \sin\gamma z_c \sin\gamma(1-z_c)}\,\Lambda^{-1/4}\,, \qquad \Lambda \to \infty\,, \tag{4.17}$$

or by (3.13)

$$s \sim \frac{\gamma|\sin\gamma|(kq)^{1/2}}{3.0065\ \sin\gamma z_c \sin\gamma(1-z_c)}\,\Lambda^{-3/4}, \qquad \Lambda\to\infty. \tag{4.18}$$

As an example, suppose that

$$q = \tfrac{3}{2}\pi, \qquad k_x = k_y = 1. \tag{4.19}$$

Then $z_c = \frac{1}{2}$, and we obtain from (4.17) and (4.18)

$$p \sim \frac{0.93057}{\Lambda^{1/4}}, \quad s \sim \frac{6.2016}{\Lambda^{3/4}}, \quad \Lambda\to\infty. \tag{4.20, 4.21}$$

For $\Lambda = 10^6$ these give

$$p \doteqdot 0.029427, \qquad s \doteqdot 1.9611\ 10^{-4}, \tag{4.22, 4.23}$$

the latter of which should be compared with the numerically determined value of $s = 1.6549\ 10^{-4}$.

Despite the small value (4.22) of p, the error (4.23) is a surprisingly large 20%. There are three reasons for this. First, our expansion is in powers of δ, i.e. in powers of $\Lambda^{-1/4}$; see (3.14). It is $\Lambda^{-1/4}$, and not Λ^{-1}, that measures the approach to the asymptotic limit $\Lambda\to\infty$. For $\Lambda = 10^6$, $\Lambda^{-1/4}$ is only about 0.032. Second, (3.45) gives only the first term in the expansion of the critical layer solution of (3.12) is powers of p. This particular source of error could be remedied by solving (3.12) numerically for arbitrary p. This would, however, be pointless because of the third, and most serious, source of error. Equation (3.12) is derived from the full equation (3.10) by retaining only the first nonzero term in the expansion (3.6) of F. An error of relative order δ in s enters instantly. A numerical study of the present case (4.19) has shown that, in the next order, (4.21) is replaced by

$$s = \frac{6.2016}{\Lambda^{3/4}} - \frac{30.58}{\Lambda}, \tag{4.24}$$

and this gives $s = 1.6553\ 10^{-4}$ for $\Lambda = 10^6$, which is in much better agreement with the numerically determined value $s = 1.6549\ 10^{-4}$. The basis for (4.25) is shown in Table 2.

The development of a critical layer structure around $z = z_c = \frac{1}{2}$ is clearly seen in Figures 2–5 in which $b_z, j_z, -iv_z, -i\omega_z$ are shown for $\Lambda = 10^3$, 10^4, 10^5 and 10^6. Figures 5, for ω_z, are particularly striking. Also to be discerned in several of these figures are the boundary layers, of thickness $O(\Lambda^{-1/2})$, adjacent to $z = 0$ and $z = 1$, but which affect s and the instability only passively, i.e. in no essential way.

Figures 6–9 show further comparisons between the solutions for $\Lambda = 10^4$ of the full equations (2.16)–(2.19), and the asymptotic theory. In panels (a) and (b) in each of these figures, the numerical solutions are compared with the mainstream solutions, which for $b_z^{(0)}$ is given by (4.14) and which for the remaining functions are given by the $\Lambda = \infty$ forms of (2.16)–(2.19), namely

$$j_z^{(0)} = -qb_z^{(0)} + \frac{s}{F}D\left(\frac{b_z^{(0)}}{F}\right), \quad -iv_z^{(0)} = -s\left(\frac{b_z^{(0)}}{F}\right), \quad -i\omega_z^{(0)} = -\frac{s^2}{F^2}D\left(\frac{b_z^{(0)}}{F}\right). \tag{4.25}$$

Although the similarities between panels (b) and (c) are striking in each case, a detailed comparison is impossible for two reasons. First, it should not be forgotten that, according to the analysis of Section 3, the solutions of the critical layer equations are non-unique; an arbitrary multiple of $w_2 = \zeta$ can be added to b_z. The addition of $\bar{A}\delta\zeta$ [where $\bar{A} = \frac{1}{2}(A_+ + A_-)$; see (3.8)] leaves ω_z and j_z unaltered to leading order in the critical layer, but adds $-i\bar{A}pF_c'\delta^2$ to v_z, i.e. it displaces the zero of $-iv_z$ at $\zeta = 0$ by $-s\bar{A}/F_c'$; see $(4.25)_2$. Since $\bar{A}$ is almost zero in the present, almost symmetric case, this displacement is not apparent in panel 8(b)[4]. Second, in the critical layer scaling (3.11) — see also (B9) later — $b_z = O(1)$ but $j_z = O(\delta^{-1})$ to leading order. In the next approximation, correction terms are added that are $O(\delta)$ and $O(1)$, respectively. The fact that j_z is unaffected to leading order by the addition of $\bar{A}\delta\zeta$ to b_z means that j_z is in error by $O(1)$, rather than by $O(\delta^{-1})$. But this error cannot be derived from the analysis of Section 3, although its existence is clearly seen when panels 7(a) and (b) are compared with panel 7(c).

We now turn to the case (iii) of two critical points. In place of (4.15) we now have, for some λ_1/λ_2,

$$b_z^{(0)} = \begin{cases} \lambda_1 \sin \gamma z / \sin \gamma z_{c1}\,, & \text{for } 0 \le z \le z_{c1}\,; \\ \lambda_2 \sin \gamma(1-z)/\sin\gamma(1-z_{c2})\,, & \text{for } z_{c2} \le z \le 1\,; \\ [\lambda_1 \sin\gamma(z_{c2}-z) + \lambda_2 \sin\gamma(z-z_{c1})]/\sin\gamma(z_{c2}-z_{c1})\,, & \text{for } z_{c1} < z < z_{c2}\,. \end{cases} \tag{4.26}$$

From each critical point we get one expression for Δ, namely

$$\left[\frac{Db_z^{(0)}}{b_z^{(0)}}\right]_{z_{c1}} = \gamma\left[\frac{\lambda_2}{\lambda_1}\mathrm{cosec}\gamma(z_{c2}-z_{c1}) - \cot\gamma(z_{c2}-z_{c1}) - \cot\gamma z_{c1}\right], \tag{4.27}_1$$

$$\left[\frac{Db_z^{(0)}}{b_z^{(0)}}\right]_{z_{c2}} = \gamma\left[\frac{\lambda_1}{\lambda_2}\mathrm{cosec}\gamma(z_{c2}-z_{c1}) - \cot\gamma(z_{c2}-z_{c1}) - \cot\gamma(1-z_{c2})\right]. \tag{4.27}_2$$

Since δ is the same for each boundary layer by (3.14) and (4.10), these two expression must both equal $2A/\delta$, and therefore must be equal to each other, so that

$$\frac{\lambda_1}{\lambda_2} - \frac{\lambda_2}{\lambda_1} = \frac{\sin(\gamma\pi/q)\sin\gamma(z_{c1}+z_{c2}-1)}{\sin\gamma z_{c1}\sin\gamma(1-z_{c2})}\,, \tag{4.28}$$

$$\Delta = \frac{\gamma}{2\sin(\gamma\pi/q)\sin\gamma z_{c1}\sin\gamma(1-z_{c2})} \cdot \left\{\left[(\sin(\gamma\pi/q)\sin\gamma(z_{c1}+z_{c2}-1))^2 + (2\sin\gamma z_{c1}\sin\gamma(1-z_{c2}))^2\right]^{1/2} + \cos\gamma - \cos(\gamma\pi/q)\cos\gamma(z_{c1}-z_{c2}-1)\right\}. \tag{4.29}$$

Equating this to $2A/\delta = 3.0065p/\delta = 3.0065s\Lambda\delta$ with $\delta = (qk)^{-1/2}\Lambda^{-1/4}$, we obtain p and δ as before.

[4]See, however, the displacement of v_z away from zero at the $z = \frac{1}{6}$ critical point in Figures 13(c) and 13(d) below.

For example, if

$$q = \tfrac{3}{2}\pi\,, \qquad k_x = -k_y = 1\,, \tag{4.30}$$

then $z_{c1} = \frac{1}{6}$ and $z_{c2} = \frac{5}{6}$. By (4.28) and (4.29), $\lambda_1 = \lambda_2$ and

$$\Delta = -\frac{2\gamma \sin \frac{1}{3}\gamma \cos \frac{1}{2}\gamma}{\sin \frac{2}{3}\gamma \sin \frac{1}{6}\gamma} \doteq 57.143\,, \tag{4.31}$$

since $\gamma \approx 4.4952$. So we obtain

$$p \sim \frac{7.3624}{\Lambda^{1/4}}\,, \qquad s \sim \frac{49.065}{\Lambda^{3/4}}\,, \qquad \Lambda \to \infty\,. \tag{4.32, 4.33}$$

For $\Lambda = 10^6$ these give

$$p = 0.23282\,, \qquad s = 1.5516\ 10^{-3}\,, \tag{4.34, 4.35}$$

the latter of which should be compared with the numerically determined value of $s = 1.1013\ 10^{-3}$. The agreement is not as good as in the case of one critical layer; the error is about 40%. This may be attributed to the reasons given below (4.23) combined with the fact that p given by (4.34) is larger than the p for the earlier case (4.22).

It is noteworthy how much greater the growth rate (4.35) is than (4.23). This is because two critical layers are twice as effective as one in reconnecting field lines of $\mathbf{B}_0$ and converting their magnetic energy into perturbation energy.

5. Numerical Results

We carried out extensive numerical integrations of the basic equations (2.16)–(2.20), both for finite values of Λ and, in a suitably scaled form, for $\Lambda = \infty$, i.e. for the critical layer structure. We shall postpone until Appendix B the description of the numerical techniques we employed and the tests of accuracy that we applied. Here we describe only our principal findings.

For every choice of $\mathbf{k}$, Λ and α, our programs located both the real and complex eigenvalues s. Although complex s were found, we discovered that in all cases the most unstable mode (i.e. the one for which $\mathrm{Re}(s)$ is greatest) is direct. In our discussion below, we focus on this real eigenvalue alone.

We always adopted (1.2) for $\mathbf{B}_0$. We investigated three cases:

$$q = \tfrac{1}{2}\pi\,, \qquad q = \tfrac{3}{2}\pi\,, \qquad q = 2\pi\,. \tag{5.1}$$

In the first of these we were unsuccessful in locating any $\mathbf{k}$ or Λ for which $s > 0$. We conjecture therefore that unstable modes do not exist when $q = \frac{1}{2}\pi$. This conclusion is consistent with the results of the asymptotic analysis developed in Sections 3 and 4.

We subjected the case $q = \frac{3}{2}\pi$ to special scrutiny. We searched for the maximum growth rate, $s_c(\Lambda)$, over the range $0 < \Lambda < 4000$, i.e. we sought, for a number of values of Λ, the value of $\mathbf{k}(= \mathbf{k}_c(\Lambda)$, say) for which $s(\mathbf{k}, \Lambda)$ is a maximum, and for which therefore

$$(\nabla_{\mathbf{k}} s)_c = 0\,. \tag{5.2}$$

There were two such local maxima, which we call 'mode 1' and 'mode 2'. As Λ is increased from zero, 'mode 1' is the first to become unstable, s_c becoming positive at $\Lambda = \Lambda_c \approx 22.17$. As Λ is increased further, mode 2 becomes the more unstable; see Figure 10 where $s_c(\Lambda)$ is plotted for both modes.

Of particular interest is the fact that, as Λ increases, $\mathbf{k}_c$ evolves in such a way that one of the two critical levels approaches a boundary, that critical layer eventually merging with the boundary layer. At that stage, the asymptotic analysis of Section 3 becomes invalid, and it is not even certain that s_c is proportional to $\Lambda^{-3/4}$, as $\Lambda \to \infty$, though it clearly cannot tend to zero more rapidly than that. In the case of mode 1, it is the critical layer at $z = z_{c2}$ that moves into the boundary layer at $z = 1$; in the case of mode 2, it is the critical layer at $z = z_{c1}$ that moves to $z = 0$; see Table 3.

The evolution of the eigenfunction for $\mathbf{k} = \mathbf{k}_c$ is shown as Λ increases in Figures 11–14 for mode 1. The development of the critical layer at $z = z_{c1}$ near $z = \frac{1}{3}$ is apparent, while at the same time the approach of the critical layer at $z = z_{c2}$ towards $z = 1$ is obvious.

When $q = 2\pi$ there are always two critical layers in the interval. Because of the greater shearing of $\mathbf{B}_0$, the growth rate of the instability is always larger than when $q = \frac{3}{2}\pi$. For instance Λ_c is 16.78, instead of 22.17 for $q = \frac{3}{2}\pi$. The maximum attainable growth rate is 0.3435, instead of 0.1140 for $q = \frac{3}{2}\pi$. When $q = 2\pi$, mode 1 is always more unstable than mode 2.

6. Conclusions

In this paper we have studied a classical phenomenon in plasma physics: resistive instabilities. We have had in mind, however, geophysical and astrophysical systems which, though in principle prone to such instabilities, are rotating rapidly, and in which therefore Coriolis forces greatly exceed inertial forces. Such systems are generally geometrically complicated, but we have felt that, in a first analysis, we should study the canonical example of tearing: the magnetic instability of the sheet pinch.

We have found that the tearing mode is strongly suppressed by rotation; the growth rate of the instability is only $O(\tau_\eta^{-3/4}\tau_s^{-1/4})$, where $\tau_s = 2\Omega\mu\rho L^2/\mathcal{B}^2$ is the relevant dynamical timescale and $\tau_\eta = \mu\sigma L^2$ is the diffusive timescale for a field of strength $\mathcal{B}$ and characteristic scale L. This may be compared with the $O(\tau_\eta^{-3/5}\tau_A^{-2/5})$ growth rate of classical theory, where $\tau_A = L/V_A$ is the appropriate dynamical timescale when inertial forces dominate Coriolis forces; V_A is the Alfvén velocity. The ratio of these two growth rates is $\Lambda^{-3/20}(V_A/\Omega L)^{2/5}$, where $\Omega L \gg V_A$ when rotation is large. Instability can then only arise if the conductivity of the fluid is sufficiently high, i.e. if the Elsasser number, $\Lambda = \sigma\mathcal{B}^2/2\Omega\rho$ is $O(1)$. It follows that when tearing occurs in a rapidly rotating fluid, the instability grows much more slowly than it would in a non-rotating fluid.

We have found that, when $\Lambda \to \infty$, the structure of the tearing mode consists of "exterior" regions in which the solution satisfies, to a first approximation, the equations governing an ideal (perfectly conducting) fluid, and "interior" regions of two types: boundary layers of thickness $O(L\Lambda^{-1/2})$ at the walls, and critical layers of thickness $O(L\Lambda^{-1/4})$ surrounding critical levels (if any), at which the perturbation is of interchange type ($\mathbf{k}.\mathbf{B}_0 = 0$). We have studied in detail the case in which the critical layers and boundary layers do not overlap. In this case, the boundary layers are completely passive (i.e.

do not influence the growth rate to leading order); the instability draws its energy from reconnection within the critical layers. We have presented numerical evidence, however, that energy is extracted with slightly greater efficiency when a boundary lies asymptotically within a critical layer, for in this case the growth rate is slightly larger, so that the the mode of maximum instability occurs when a critical level is at a wall.

We have also shown that the sheet pinch is more unstable when $\mathbf{J}_0 \times \mathbf{B}_0 / \mathbf{J}_0 . \mathbf{B}_0$ is antiparallel to $\mathbf{\Omega}$ in the equilibrium state than when it is parallel.

Acknowledgements

We are grateful to our colleague, Nick Grossman, for pointing out to us how Mellin transforms could be elegantly used to remove gamma functions from (3.43), so making it possible to obtain (3.44), and also to our colleague Heinz Kreiss for his advice on the integrations described in Appendix B. We thank Dr. Steve Moler for supplying the subroutines we used in applying the QZ algorithm to our numerical work. One of us (WK) is grateful to the National Science Foundation for support under grant EAR-8846267; the other of us (PHR) thanks NSF for the same reason, and also thanks the Office of Naval Research for partial support under a URI grant N00014-86-K-0641.

References

Acheson, D.J. "Hydromagnetic wavelike instabilities in a rapidly rotating stratified fluid," *J. Fluid Mech.* **61**, 609–624 (1973).

Barston, E.M. "Stability of the resistive sheet pinch," *Phys. Fluids* **12**, 2162–2174 (1969).

Braginsky, S.I. "Magnetohydrodynamics of the Earth's core," *Geomag. Aeron.* **4**, 698–712 (1964).

Braginsky, S.I. "Magnetic waves in the Earth's core," *Geomag. Aeron.* **7**, 851–859 (1967).

Braginsky, S.I. "Magnetic waves in the Earth's core II," *Geophys. Astrophys. Fluid Dynam.* **14**, 189–208 (1980).

Fearn, D.R. "Differential rotation and thermal convection in a rapidly rotating hydromagnetic system," *Geophys. Astrophys. Fluid Dynam.* **49**, 173–193 (1989).

Fearn, D.R. and Proctor, M.R.E. "Hydromagnetic waves in a differentially rotating sphere," *J. Fluid Mech.* **128**, 1–20 (1983a).

Fearn, D.R. and Proctor, M.R.E. "The stabilising role of differential rotation on hydromagnetic waves," *J. Fluid Mech.* **128**, 21–36 (1983b).

Furth, H.P., Killeen, J. and Rosenbluth, M.N. "Finite resistive instabilities of a sheet pinch," *Phys. Fluids* **6**, 459–484 (1963).

Golub, G.H. and van Loan C.F. "Matrix Computations", 2nd Edition. Johns Hopkins University Press, Baltimore (1989).

Hide, R. "A note on short-term core-mantle coupling, geomagnetic secular variation impulses, and potential magnetic field invariants as Lagrangean tracers of core motions," *Phys. Earth planet. Inter.* **39**, 297–300 (1985).

Kreiss, H.-O. "Difference approximations for boundary and eigenvalue problems for ordinary differential equations," *Math. of Comp.* **26**, 605-624 (1972).

Moler, C.B. and Stewart, G.W. "An algorithm for generalized matrix eigenvalue problems," *SIAM J. Numer. Anal.* **10**, 241–256 (1973).

Oberhettinger, F. *Tables of Mellin Transforms*, Springer, Heidelberg (1974).

Roberts, P.H. *An Introduction to Magnetohydrodynamics*, Longmans, Edinburgh (1969).

APPENDIX A: BEHAVIOR OF b_z AT THE EDGE OF THE CRITICAL LAYER.

We have seen in Section 3 that the solution at the edge of the critical layer is determined by the behavior as $\zeta \to +\infty$ of

$$W = \sum_{m=0}^{\infty} \frac{(-1)^m \left(\zeta^2 \mathrm{e}^{-i\pi/4}/8\right)^m}{\Gamma\left(\frac{m}{4}+\frac{1}{4}\right)\Gamma\left(\frac{m}{4}+\frac{3}{8}\right)\Gamma\left(\frac{m}{4}+\frac{5}{8}\right)\Gamma\left(\frac{m}{4}+1\right)\left(\frac{m}{4}-\frac{1}{8}\right)}. \tag{A1}$$

The leading term in its asymptotic expansion is $K\zeta$, where K is to be found. To this end we write

$$K = \left(\frac{dW}{d\zeta}\right)_{\zeta=\infty} = \int_0^{\infty} \frac{d^2W}{d\zeta^2} d\zeta = -2\sqrt{2}\mathrm{e}^{-i\pi/4} \int_0^{\infty} P_0 \frac{dz}{z^{7/8}} = -2\sqrt{2}\mathrm{e}^{-i\pi/4} \mathcal{M}\left(P_0; \tfrac{1}{8}\right), \tag{A2}$$

where $\mathcal{M}(P_0; s)$ is the Mellin transform of

$$P_0 = \sum_{m=0}^{\infty} \frac{(-1)^m \mathrm{e}^{-i\pi m/4} z^{m/4}}{\Gamma\left(\frac{m}{4}+\frac{1}{4}\right)\Gamma\left(\frac{m}{4}+\frac{1}{2}\right)\Gamma\left(\frac{m}{4}+\frac{5}{8}\right)\Gamma\left(\frac{m}{4}+\frac{7}{8}\right)}. \tag{A3}$$

The evaluation of $\mathcal{M}(P_0; s)$ rests on the result that, if $\mathcal{L}(P, t)$ is the Laplace transform of a function $P(z)$, then

$$\mathcal{M}\left[\mathcal{L}\left(z^{\nu-1}P(z), t\right); s\right] = \Gamma(s)\mathcal{M}\left[P(z); \nu - s\right]; \tag{A4}$$

e.g. see the result (o′) on p3 of Oberhettinger (1974). Evidently

$$\mathcal{L}\left(z^{\nu-1}P_0(z), t\right) = \sum_{m=0}^{\infty} \frac{(-1)^m \mathrm{e}^{-i\pi m/4}}{\Gamma\left(\frac{m}{4}+\frac{1}{4}\right)\Gamma\left(\frac{m}{4}+\frac{1}{2}\right)\Gamma\left(\frac{m}{4}+\frac{5}{8}\right)\Gamma\left(\frac{m}{4}+\frac{7}{8}\right)} \frac{\Gamma\left(\frac{m}{4}+\nu\right)}{t^{\frac{m}{4}+\nu}}, \tag{A5}$$

a series that converges for all $|t| > 0$. Taking the Mellin transform of (A5), we obtain

$$\mathcal{M}\left[\mathcal{L}\left(z^{\nu-1}P_0(z), t\right); s\right] = \mathcal{M}\left[P_1(z); \nu - s\right], \tag{A6}$$

where

$$P_1 = \sum_{m=0}^{\infty} \frac{(-1)^m \Gamma\left(\frac{m}{4}+\nu\right) \mathrm{e}^{-i\pi m/4} z^{m/4}}{\Gamma\left(\frac{m}{4}+\frac{1}{4}\right)\Gamma\left(\frac{m}{4}+\frac{1}{2}\right)\Gamma\left(\frac{m}{4}+\frac{5}{8}\right)\Gamma\left(\frac{m}{4}+\frac{7}{8}\right)}. \tag{A7}$$

Thus, by (A4)

$$\mathcal{M}(P_0; s) = \frac{\mathcal{M}(P_1; s)}{\Gamma(\nu - s)}. \tag{A8}$$

By choosing $\nu = \frac{1}{4}$, the first of the gamma functions that appears in P_0 is eliminated from the denominator of (A7).

Continue this process three times more, eliminating all gamma functions from the denominator of series (A3), so obtaining

$$\mathcal{M}(P_0; s) = \frac{\mathcal{M}(P_4; s)}{\Gamma(\frac{1}{4}-s)\Gamma(\frac{1}{2}-s)\Gamma(\frac{5}{8}-s)\Gamma(\frac{7}{8}-s)}, \tag{A9}$$

where

$$P_4 \;=\; \sum_{m=0}^{\infty} (-1)^m \mathrm{e}^{-i\pi m/4} z^{m/4} \;=\; \frac{1}{1 \,+\, \mathrm{e}^{-i\pi/4} z^{1/4}}. \tag{A10}$$

Clearly, from the definition of the Mellin transform,

$$\mathcal{M}(P_4;\, s) \;=\; \int_0^{\infty} \frac{t^{s\,-1} dt}{1 \,+\, \mathrm{e}^{-i\pi/4} t^{1/4}} \;=\; 4\pi \mathrm{e}^{i\pi s} \mathrm{cosec} 4\pi s. \tag{A11}$$

By (A9) and (A11), we now have

$$\mathcal{M}(P_0;\, s) \;=\; \frac{4\pi \mathrm{e}^{i\pi s} \mathrm{cosec} 4\pi s}{\Gamma(\frac{1}{4} \,-\, s)\Gamma(\frac{1}{2} \,-\, s)\Gamma(\frac{5}{8} \,-\, s)\Gamma(\frac{7}{8} \,-\, s)}. \tag{A12}$$

Returning to (A2), we finally obtain

$$K \;=\; -\frac{8(2\pi)^{1/2} \mathrm{e}^{-i\pi/8}}{\Gamma\left(\frac{1}{8}\right) \Gamma\left(\frac{3}{8}\right) \Gamma\left(\frac{3}{4}\right)}. \tag{A13}$$

To make use of this result, we appeal to (3.20), (3.30), (3.41) and (3.42), and obtain

$$A \;=\; A_p p \;+\; A'_\alpha \alpha, \tag{A14}$$

where

$$A_p \;=\; -\tfrac{1}{8} \left(\tfrac{\pi}{2}\right)^{1/2} \Gamma\left(\tfrac{1}{4}\right) \Gamma\left(\tfrac{5}{8}\right) \Gamma\left(\tfrac{7}{8}\right) (K \,+\, K^*), \tag{A15}$$

$$A'_\alpha \;=\; \tfrac{1}{8} \left(\tfrac{\pi}{2}\right)^{1/2} \Gamma\left(\tfrac{1}{8}\right) \Gamma\left(\tfrac{3}{4}\right) \Gamma\left(\tfrac{7}{8}\right) \left[\mathrm{e}^{-i\pi/4} K \,+\, \mathrm{e}^{i\pi/4} K^*\right]. \tag{A16}$$

On substituting from (A13), we obtain (3.46) and (3.47).

It may also be noted that if, as in our representations of series (3.21) and (3.22) by integrals (3.25) and (3.26), we express series (A1) as a contour integral, using a contour of the type shown in Figures 1 and 2, the residue at the pole $s \;=\; -\frac{1}{2}$ outside the contour is, when multiplied by $-2\pi i$, equal to $K\zeta$, the minus sign arising because a distorted contour would pass round $s \;=\; -\frac{1}{2}$ in a clockwise sense.

APPENDIX B: NUMERICAL METHODS

Finite Λ

The eigenvalue problem for s posed by (2.16)–(2.19) and boundary conditions (2.21) was solved by finite difference methods. On writing

$$(f_1, f_2, f_3, f_4) \;=\; (v_z, \omega_z, ib_z, ij_z), \tag{B1}$$

these become

$$\begin{aligned}
Df_1 + \qquad\qquad & \bar{F}f_3 + \qquad\qquad & Ff_4 &= 0, && \text{(B2)}\\
-\Lambda F^2 f_1 + Df_2 + \quad & (D^2F \;-\; \Lambda s F)f_3 & &= 0, && \text{(B3)}\\
-Ff_1 + \quad & [\Lambda^{-1}(D^2 \;-\; k^2) \;-\; s]f_3 & &= 0, && \text{(B4)}\\
\bar{F}f_1 - Ff_2 + & & [\Lambda^{-1}(D^2 \;-\; k^2) \;-\; s]f_4 &= 0, && \text{(B5)}
\end{aligned}$$

and

$$f_1 \;=\; f_3 \;=\; Df_4 \;=\; 0, \qquad \text{at} \quad z \;=\; 0, 1; \tag{B6}$$

here $D \;=\; d/dz$.

The range $[0, 1]$ of integration was divided into N equal intervals of length $h \;=\; 1/N$, and the derivatives in (B2)–(B6) were replaced by centered differences; the derivatives of f_4 in (B6) were represented by right-hand and left-hand differences in the obvious way. This gave $4N + 2$ difference equations in $4N + 4$ unknowns, namely the values of the four functions f_n at the $N \;+\; 1$ grid points. The system was closed by two further relations, obtained from

$$Df_2 \;=\; 0, \qquad \text{at} \quad z \;=\; 0, 1, \tag{B7}$$

which are obvious consequences of (B3) and (B6). The values of f_n at the end points $z \;=\; 0,\, 1$ could then be eliminated and an algebraic eigenvalue problem, of the form

$$AX \;=\; sBX, \tag{B8}$$

could be posed, where A and B are banded $4(N-1) \times 4(N-1)$ matrices and X is a $1 \times 4(N-1)$ column vector consisting of the values of f_n at all grid values except those at $z \;=\; 0,\, 1$. As mentioned in Section 5, we did not presuppose that s is real, and performed all calculations in complex arithmetic.

The matrix B is singular, and (B8) therefore poses a so-called *generalized eigenvalue problem*, which can be solved by the QZ algorithm (Moler and Stewart, 1973). The advantage of this method is that it finds all nonsingular eigenvalues of (B6). It does not, however, take advantage of the banded structures of A and B. Moreover, we are really only interested in the eigenvalue, s_1, that has the largest real part. We therefore nearly always employed the inverse iteration method (e.g. Golub and van Loan, 1989). Provided both s_1 and the initial guess, μ, for s_1 are real, and provided μ is sufficiently large, inverse iteration always converges to s_1. Confirmation that the value of s_1 obtained was the one having the largest real part could always be verified by an application of the QZ algorithm.

The accuracy of the finite difference scheme leading to (B8) is $O(h^2)$. Convergence tests were carried out with the results shown in Figures 15 and 16 and Table 4.

Infinite Λ

The critical layer equation (3.12), attacked by analytic methods in Section 3, was also studied numerically. We did this by rescaling (B2)–(B5) by

$$(f_1, f_2, f_3, f_4) \rightarrow (F_c'\delta f_1, F_c' f_2, f_3, f_4/\delta), \tag{B9}$$

and then taking the limit $\Lambda \rightarrow \infty$, so obtaining

$$\begin{aligned}
Df_1 - \qquad\qquad \alpha f_3 + \qquad \zeta f_4 &= 0, && \text{(B10)}\\
-\zeta^2 f_1 + Df_2 - \qquad p\zeta f_3 \qquad\quad &= 0, && \text{(B11)}\\
-\zeta f_1 + \qquad (D^2 - p) f_3 \qquad\quad &= 0, && \text{(B12)}\\
-\alpha f_1 - \zeta f_2 + \qquad\qquad (D^2 - p) f_4 &= 0. && \text{(B13)}
\end{aligned}$$

Here $D = d/d\zeta$, where ζ is z scaled as in (3.11), the critical level itself being $\zeta = 0$; p is the scaled growth rate (3.13), and α, the magnetic helicity at the critical level, is defined by (3.15). Solutions to (B10)–(B13) must satisfy boundary conditions that follow from (3.18)–(3.10):

$$f_1(0) = 0, \quad f_3(0) = 1, \quad f_4(0) = 0, \quad Df_3(0) = 0, \tag{B14}$$

$$f_2(X) = 0, \quad Df_4(X) = 0. \tag{B15}$$

Here X is a numerical substitute for ∞; it is clear from the analysis of Section 3 that this will introduce errors of order $\zeta^{-3/2}\exp(-\zeta^2/2\sqrt{2})$. These are negligible if, as we assumed, $X = 5$. (In some cases we chose $X = 10$, and obtained the same results as in Table 1, to the accuracy shown.) The prime objective is that of evaluating $f_3(\infty)$, or effectively

$$A = f_3(X). \tag{B16}$$

Our finite difference scheme for (B10)-(B15) followed that described by Kreiss (1972), a paper in which the stability and consistency of the method is analyzed in detail.

TABLE 1
Values of $A_p(\alpha)$ and $A_\alpha(\alpha)$

α	- 10	- 5	- 2	- 1	0
$A_p(\alpha)$	- 1.8506	- 0.4067	0.7311	1.1193	1.5032
$A_\alpha(\alpha)$	- 1.8118	- 5.2505	- 3.4337	- 1.9595	0.0

α	1	2	5	10
$A_p(\alpha)$	1.8784	2.2411	3.2245	4.4179
$A_\alpha(\alpha)$	2.47101	5.4768	17.893	50.666

TABLE 2
Numerical basis of (4.25)

$\Lambda \times 10^{-6}$	$s \times 10^4$	$6.2016\Lambda^{1/4} - s\Lambda$
0.5	2.6885	30.485
1.0	1.6550	30.613
1.5	1.2424	30.675
2.0	0.8634	30.713
3.0	0.7578	30.759
4.0	0.6164	30.785
5.0	0.5249	30.801
6.0	0.4602	30.811
7.0	0.4117	30.817

TABLE 3
The most unstable modes for $q = \frac{3}{2}\pi$

Mode 1

Λ	k_{xc}	k_{yc}	$\sigma_c \times 10^4$	ζ_{c1}	ζ_{c2}
22.17	1.70987	-0.39001	0.10262	0.2857	0.9524
75.60	1.63151	-0.32520	0.11405	0.2916	0.9582
1000	1.45943	-0.21715	0.05059	0.3019	0.9686
2000	1.39553	-0.19984	0.03617	0.3032	0.9695
3000	1.35768	-0.19070	0.02942	0.3037	0.9704
4000	1.33079	-0.18578	0.02532	0.3039	0.9706

Mode 2

Λ	k_{xc}	k_{yc}	$\sigma_c \times 10^4$	ζ_{c1}	ζ_{c2}
41.5	1.51995	-1.50941	0.00557	0.1674	0.8341
125.2	1.23400	-1.41142	0.15455	0.1528	0.8191
1000	0.80384	-1.28158	0.07118	0.1189	0.7855
2000	0.67358	-1.25873	0.05001	0.1043	0.7709
3000	0.60495	-1.24294	0.04032	0.0961	0.7628
4000	0.56011	-1.22847	0.03452	0.0908	0.7574

TABLE 4
Numerical Convergence for some $q = \frac{3}{2}\pi$ cases

Fixed k. $k_x = k_y = 1, \Lambda = 10^6$

h	0.004	0.002	0.001
s	$1.6573\,10^{-4}$	$1.6554\,10^{-4}$	$1.6549\,10^{-4}$

Most Unstable Mode, $\Lambda = 2000$

h	0.004	0.002	0.001
k_{xc}	1.39567	1.39550	1.39546
k_{yc}	-0.199827	-0.199846	-0.199852
s_c	$3.6190\,10^{-2}$	$3.6169\,10^{-2}$	$3.6163\,10^{-2}$

LEGENDS FOR FIGURES

Figure 1. The contours for the integral representation of solutions of the homogeneous equation (3.17). (a) The contour C_3 for w_3 as given by (3.25), (b) the contour C_4 for w_4 as given by (3.26).

Figure 2. The function b_z for the case $k_x = k_y = 1$ for (a) $\Lambda = 10^3$, (b) $\Lambda = 10^4$, (c) $\Lambda = 10^5$ and (d) $\Lambda = 10^6$ showing the development of the asymptotic structure.

Figure 3. The function j_z for the cases shown in Figure 2.

Figure 4. The function v_z (multiplied by - i) for the cases shown in Figure 2.

Figure 5. The function ω_z (multiplied by - i) for the cases shown in Figure 2.

Figure 6. The function b_z for the case $k_x = k_y = 1$ and $\Lambda = 10^4$, (a) as computed by integration of the full equations (2.16)–(2.19) (these points are marked with a +) and compared with the mainstream from (4.20); (b) the same, but showing the critical region on an enlarged scale; (c) the result of integration of the critical layer equations, $\zeta = 0$ corresponding to the critical point itself.

Figure 7. The function j_z for the same three cases as shown in Figure 6. Here the mainstream form of j_z is obtained from (4.26).

Figure 8. The function v_z (multiplied by -i) for the cases shown in Figure 7.

Figure 9. The function ω_z (multiplied by -i) for the cases shown in Figure 7.

Figure 10. The growth rate, $s_c(\Lambda)$, for the most unstable mode, i.e. the local maxima of $s(\mathbf{k}, \Lambda)$ as a function of Λ, obtained by solving (5.2). Two such maxima exist in the case $q = \frac{3}{2}\pi$ shown: mode 1 (M_1) and mode 2 (M_2).

Figure 11. The evolution of b_z as Λ increases, shown for four values of Λ for mode 1 in the case $q = \frac{3}{2}\pi$: (a) $\Lambda = \Lambda_c = 22.17$, close to the marginal state for the tearing mode, $k_{xc} = 1.7100$, $k_{yz} = 0.3900$; (b) $\Lambda = 75.6$, close to the maximum attainable growth rate for the tearing mode, $k_{xc} = 1.6315$, $k_{yc} = -0.3252$, $\sigma_c = 0.1140$; (c) $\Lambda = 2,000$, $k_{xc} = 1.3955$, $k_{yc} = -0.1998$, $\sigma_c = 0.03617$; (d) $\Lambda = 4,000$, $k_{xc} = 1.3308$, $k_{yc} = -0.1858$, $\sigma_c = 0.02532$.

Figure 12. The evolution of j_z as Λ increases, for the cases shown in Figure 11.

Figure 13. The evolution of v_z as Λ increases, for the cases shown in Figure 11.

Figure 14. The evolution of ω_z as Λ increases, for the cases shown in Figure 11.

Figure 15. Convergence of b_z as the step size, h, is reduced; $\Lambda = 10^6$, $k_x = k_y = 1$, $q = \frac{3}{2}\pi$. Results for $h = 0.005, 0.0025$ and 0.00125 are marked by +, 0 and −, respectively. In (a) the full range $0 \leq z \leq 1$ is shown; in (b) only the vicinity of the critical point, $z_c = \frac{1}{2}$, is shown.

Figure 16. Convergence of j_z as the step size, h, is reduced; the same cases as in Figure 15.

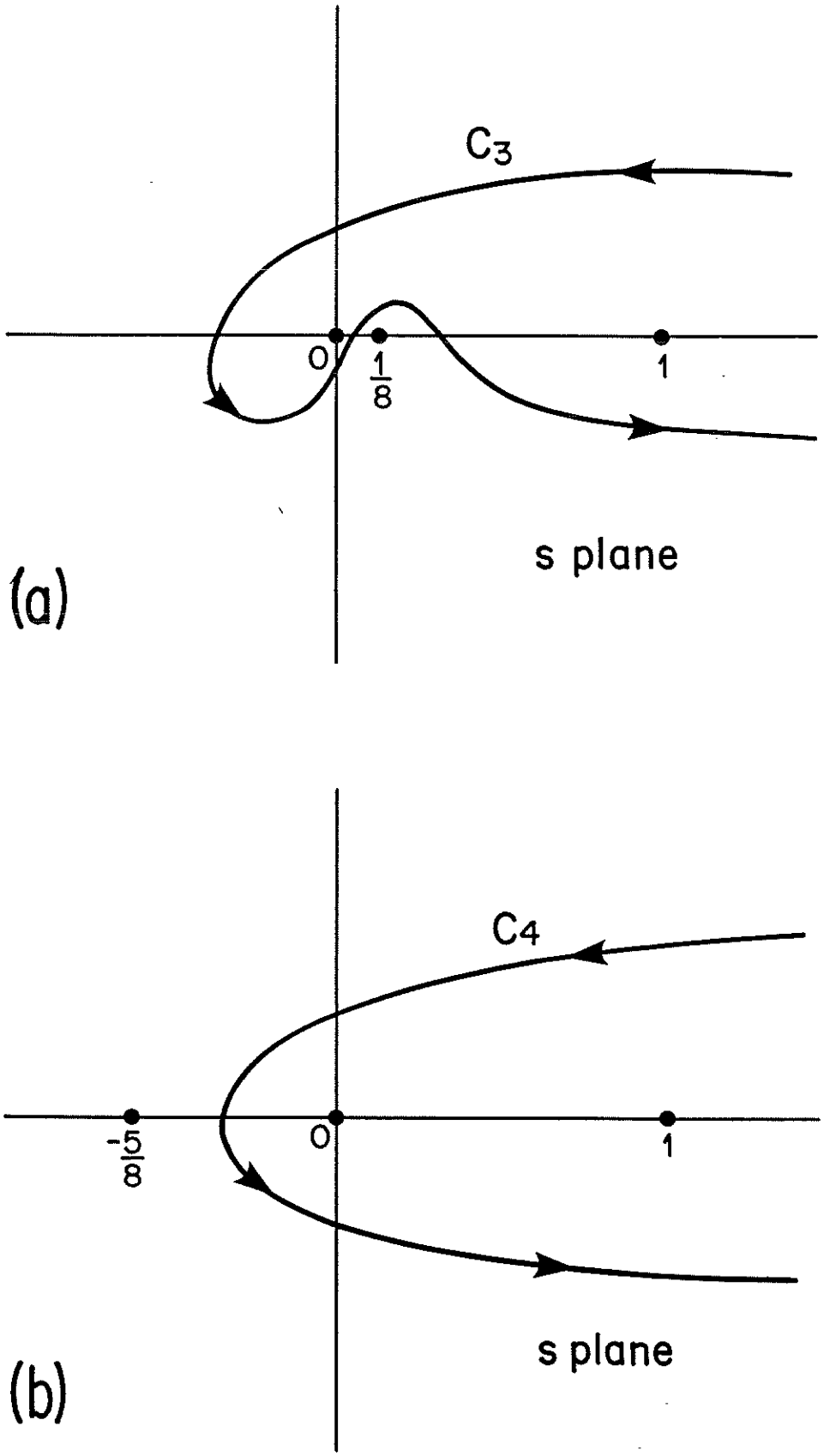

FIGURE 1. The contours for the integral representation of solutions of the homogeneous equation (3.17): (a) The contour C_3 for w_3 as given by (3.25), (b) the contour C_4 for w_4 as given by (3.26).

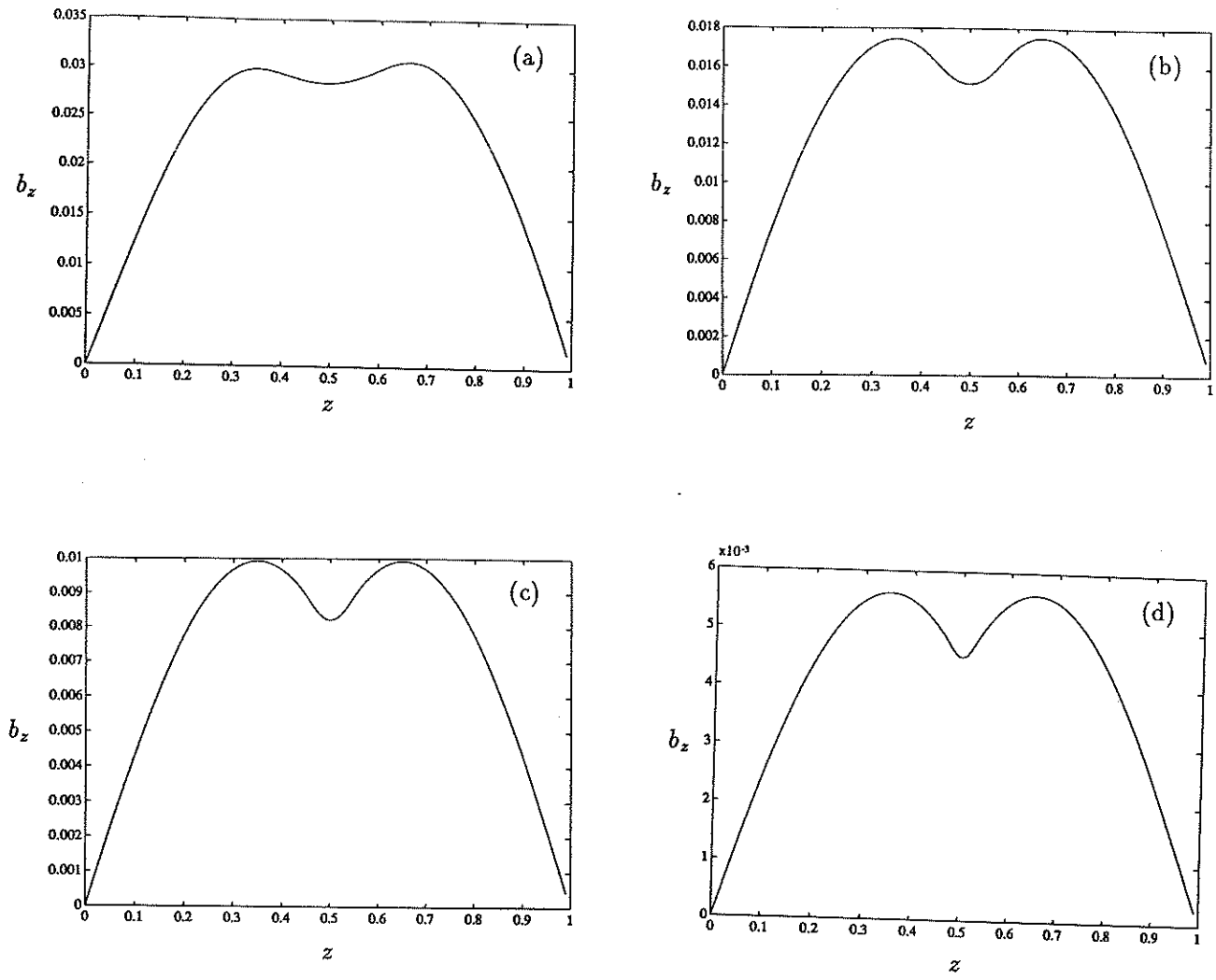

FIGURE 2. The function b_z for the case $k_x = k_y = 1$ for (a) $\Lambda = 10^3$, (b) $\Lambda = 10^4$, (c) $\Lambda = 10^5$ and (d) $\Lambda = 10^6$ showing the development of the asymptotic structure.

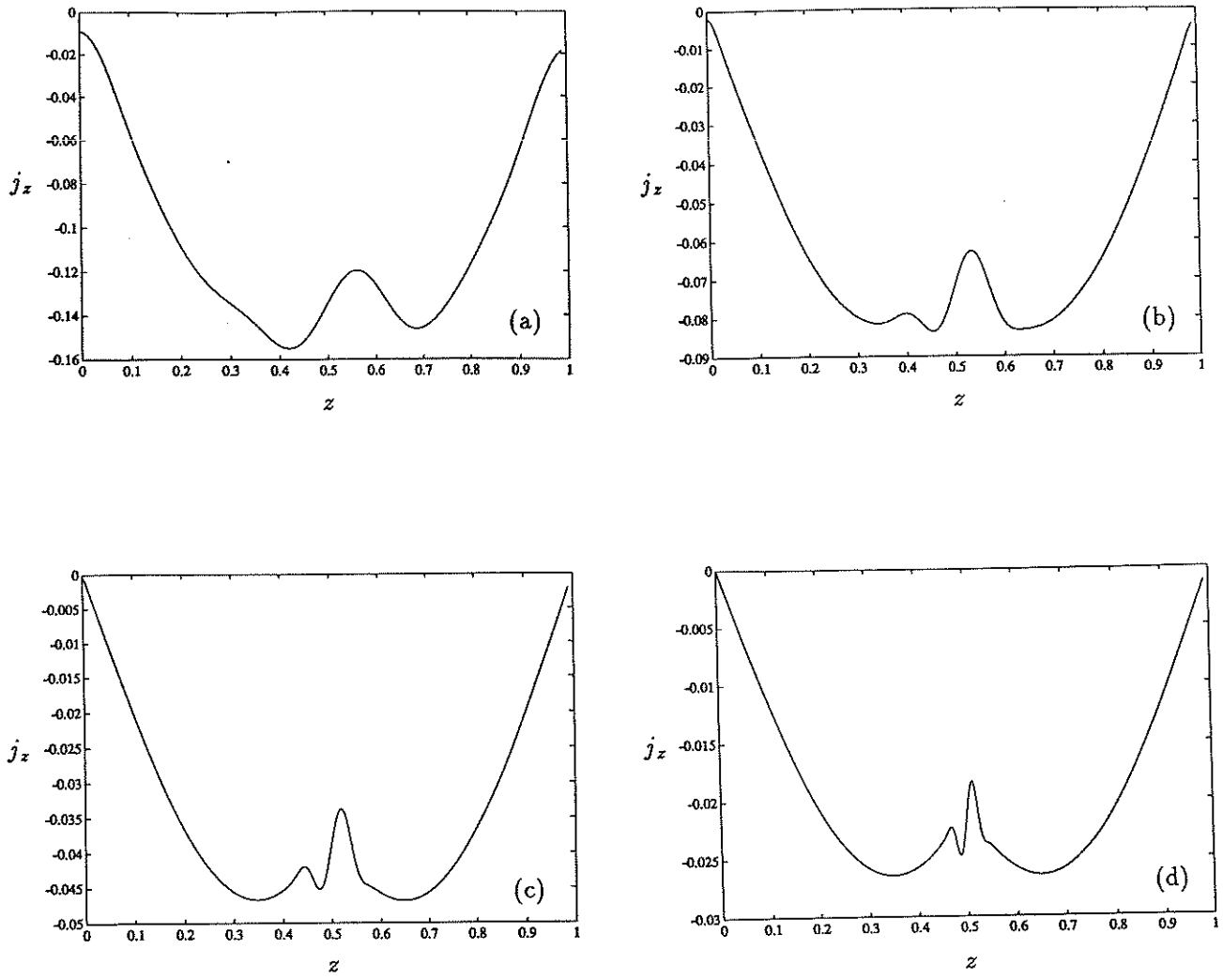

FIGURE 3. The function j_z for the cases shown in Figure 2.

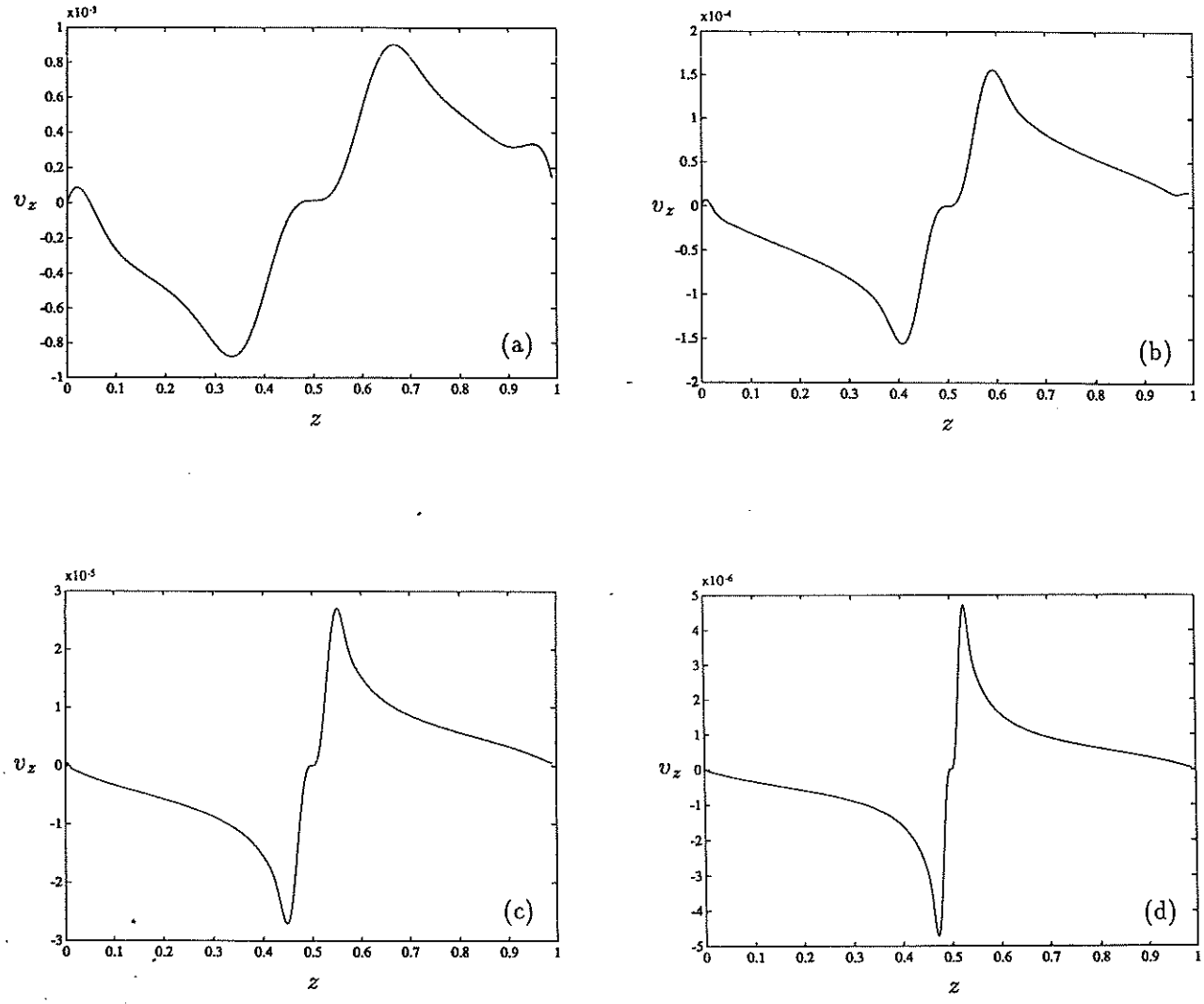

FIGURE 4. The function v_z (multiplied by - i) for the cases shown in Figure 2.

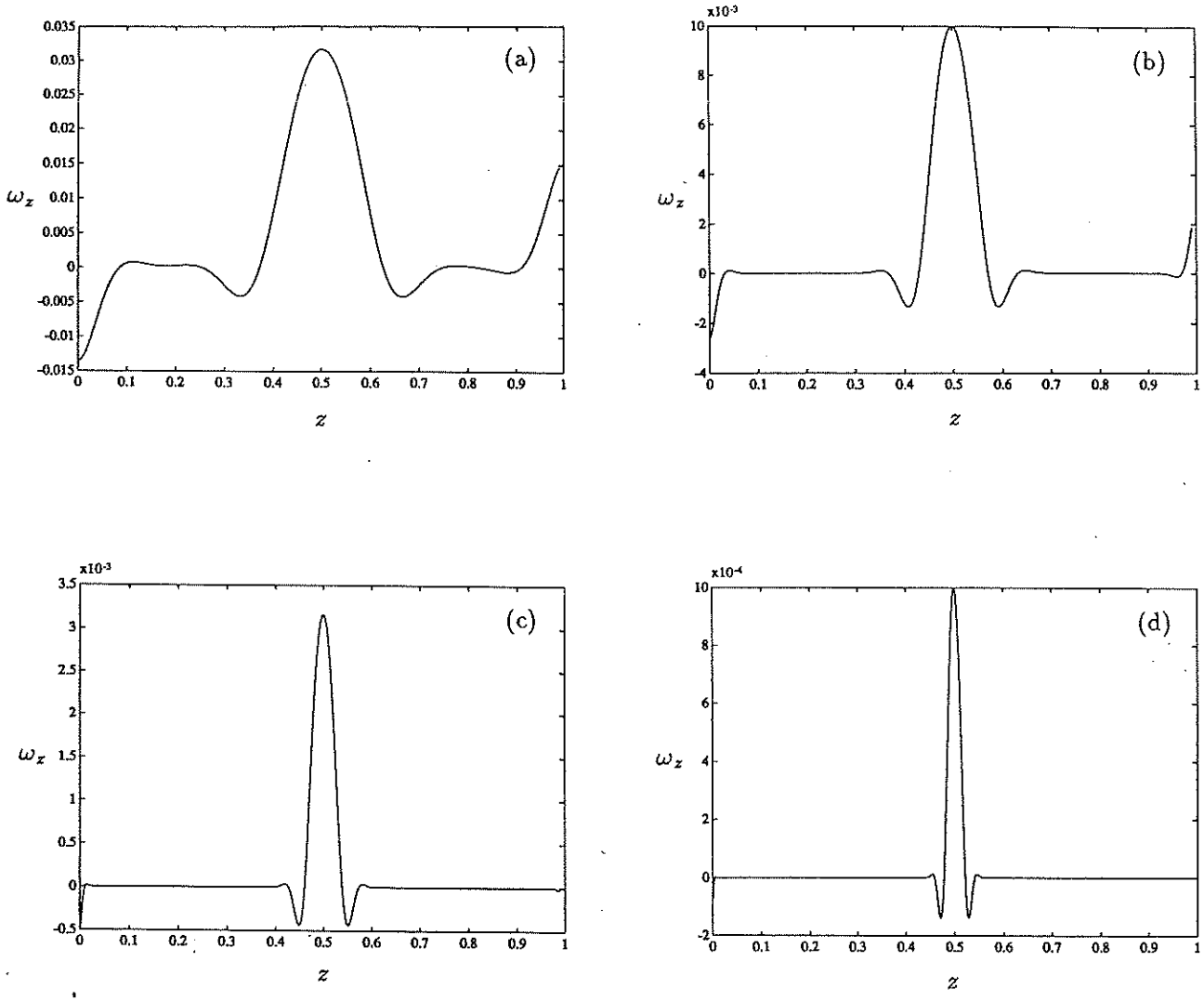

FIGURE 5. The function ω_z (multiplied by - i) for the cases shown in Figure 2.

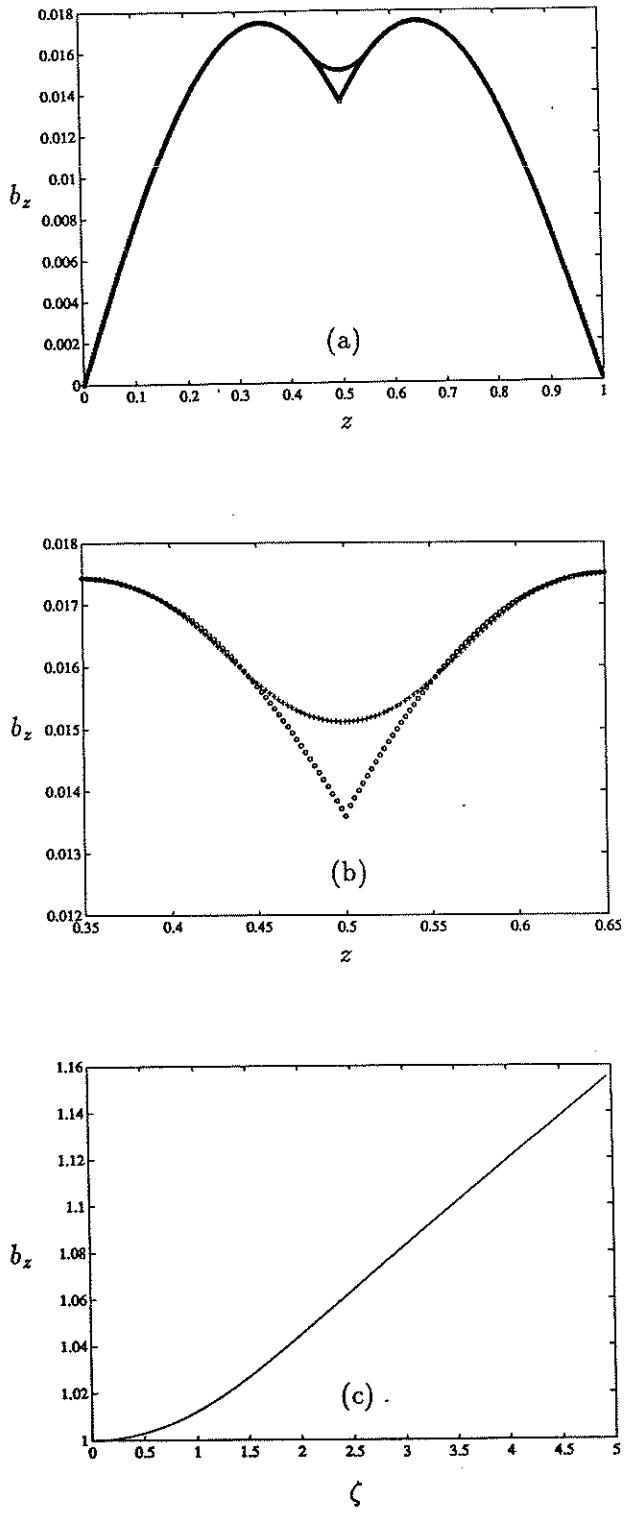

FIGURE 6. The function b_z for the case $k_x = k_y = 1$ and $\Lambda = 10^4$, (a) as computed by integration of the full equations (2.16)–(2.19) (these points are marked with a +) and compared with the mainstream form (4.20); (b) the same, but showing the critical region on an enlarged scale; (c) the result of integration of the critical layer equations, $\zeta = 0$ corresponding to the critical point itself.

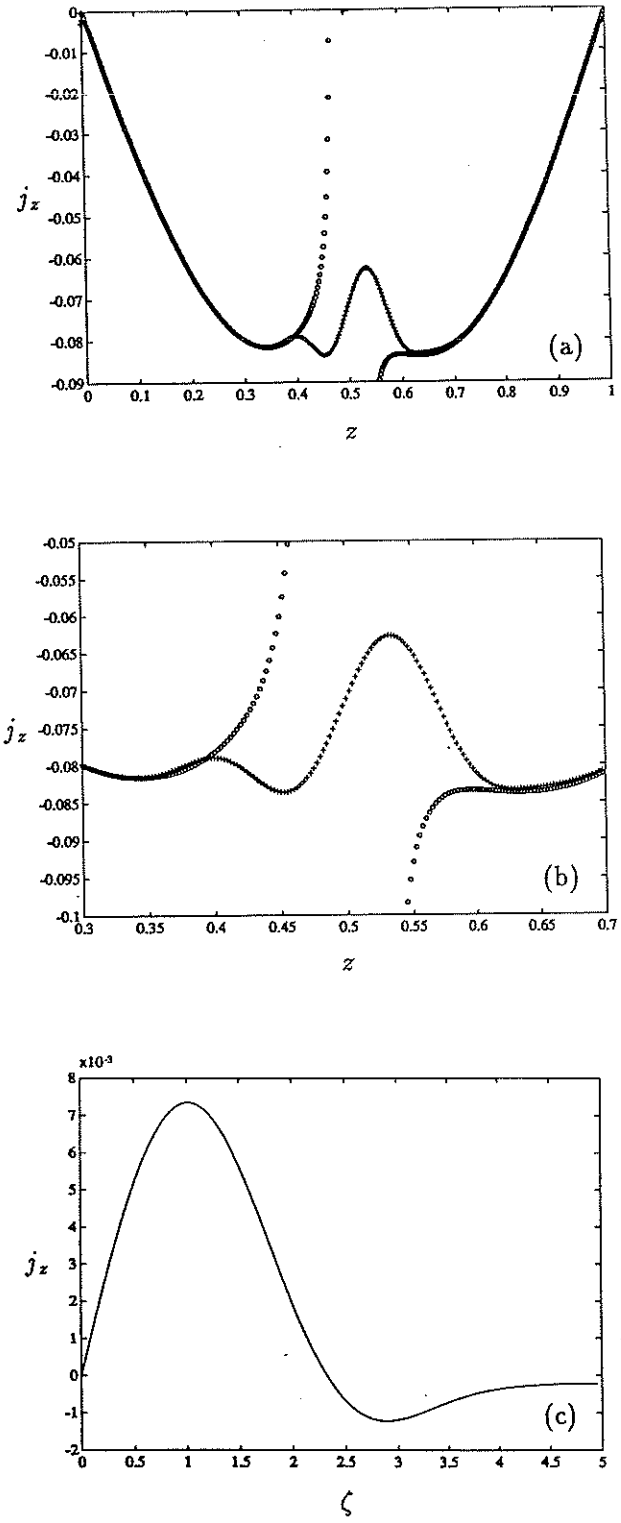

FIGURE 7. The function j_z for the same three cases as shown in Figure 6. Here the mainstream form of j_z is obtained from the b_z of Figure 6 by using (4.26).

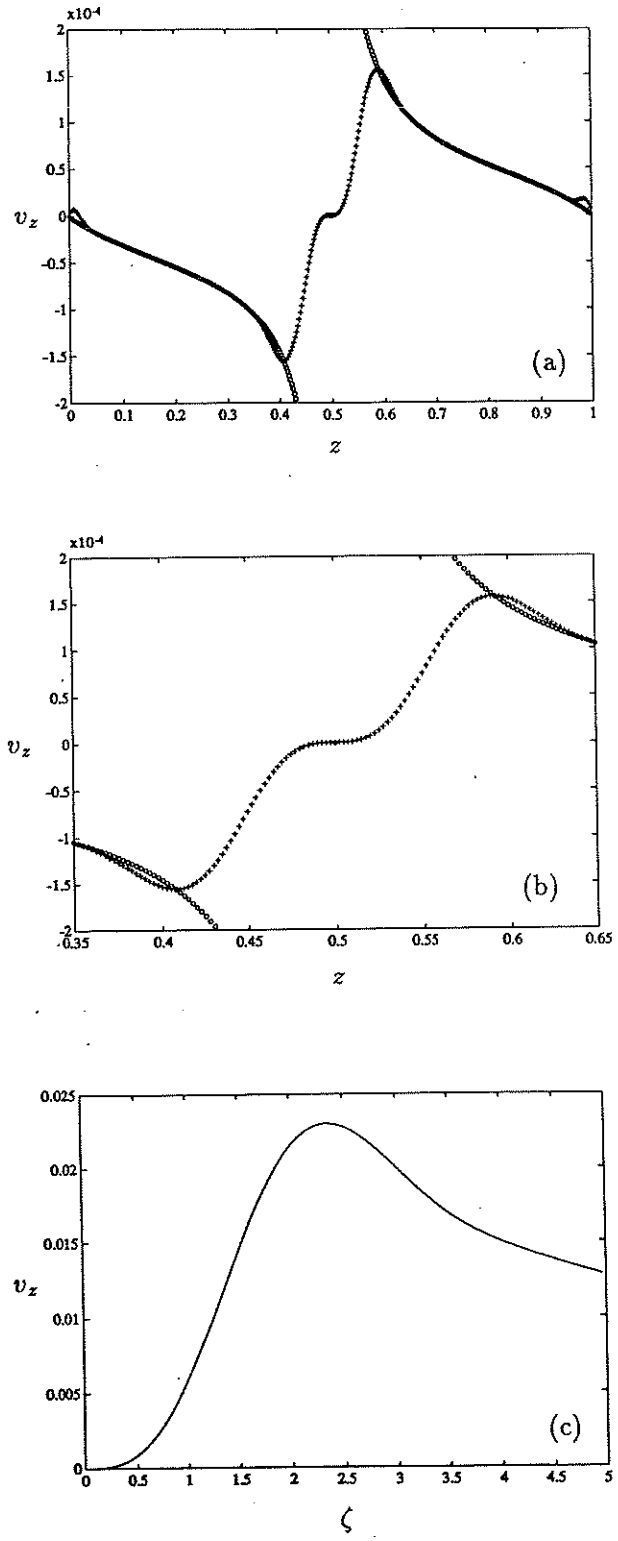

FIGURE 8. The function v_z (multiplied by -i) for the cases shown in Figure 7; see (4.26).

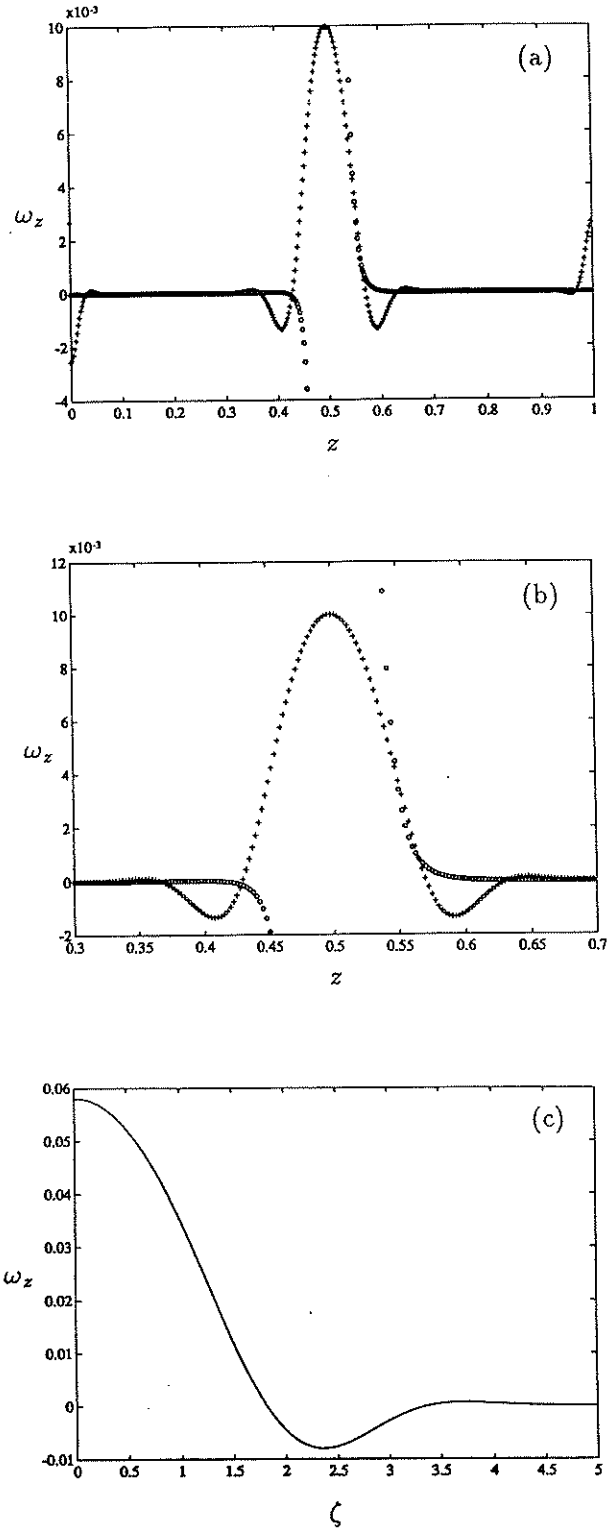

FIGURE 9. The function ω_z (multiplied by -i) for the cases shown in Figure 7; see (4.26).

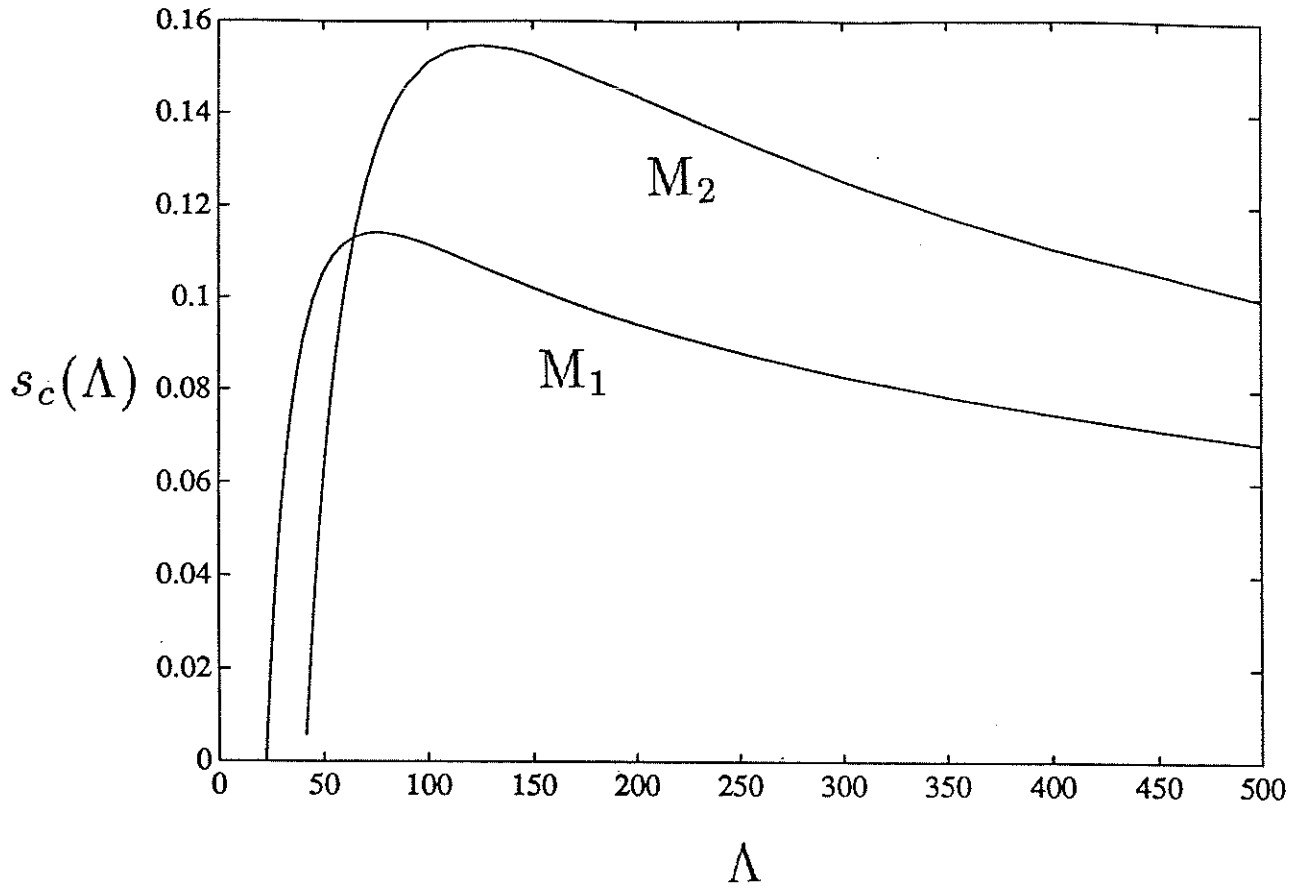

FIGURE 10. The growth rate, $s_c(\Lambda)$, for the most unstable mode, i.e. the local maxima of $s(\mathrm{k}, \Lambda)$ as functions of Λ, obtained by solving (5.2). Two such maxima exist in the case $q = \frac{3}{2}\pi$ shown: mode I (M_1) and mode II (M_2).

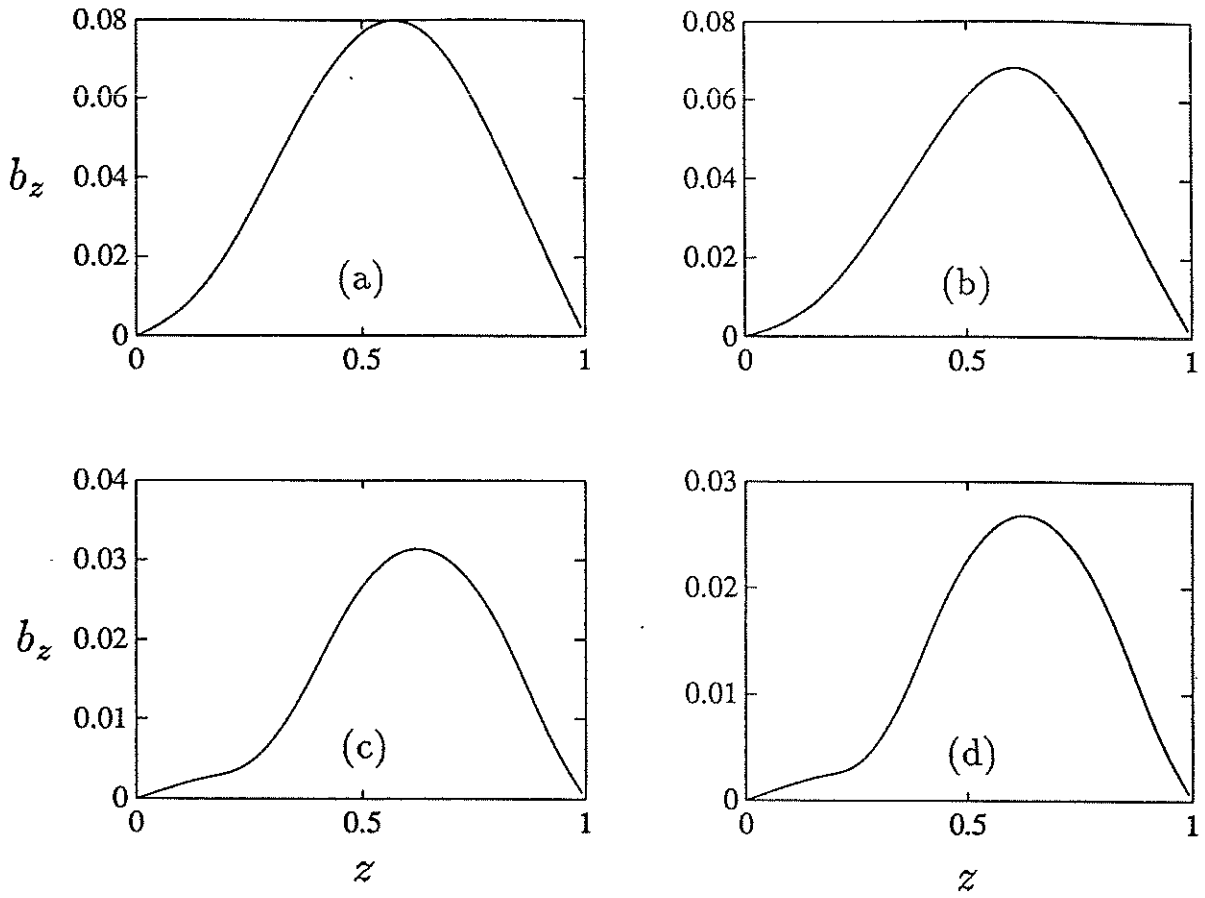

FIGURE 11. The evolution of b_z as Λ increases, shown for four values of Λ for mode I in the case $q = \frac{3}{2}\pi$: (a) $\Lambda = \Lambda_c = 22.17$, close to the marginal state for the tearing mode, $k_{xc} = 1.7100$, $k_{yz} = 0.3900$; (b) $\Lambda = 75.6$, close to the maximum attainable growth rate for the tearing mode, $k_{xc} = 1.6315$, $k_{yc} = -0.3252$, $\sigma_c = 0.1140$; (c) $\Lambda = 2,000$, $k_{xc} = 1.3955$, $k_{yc} = -0.1998$, $\sigma_c = 0.03617$; (d) $\Lambda = 4,000$, $k_{xc} = 1.3308$, $k_{yc} = -0.1858$, $\sigma_c = 0.02532$.

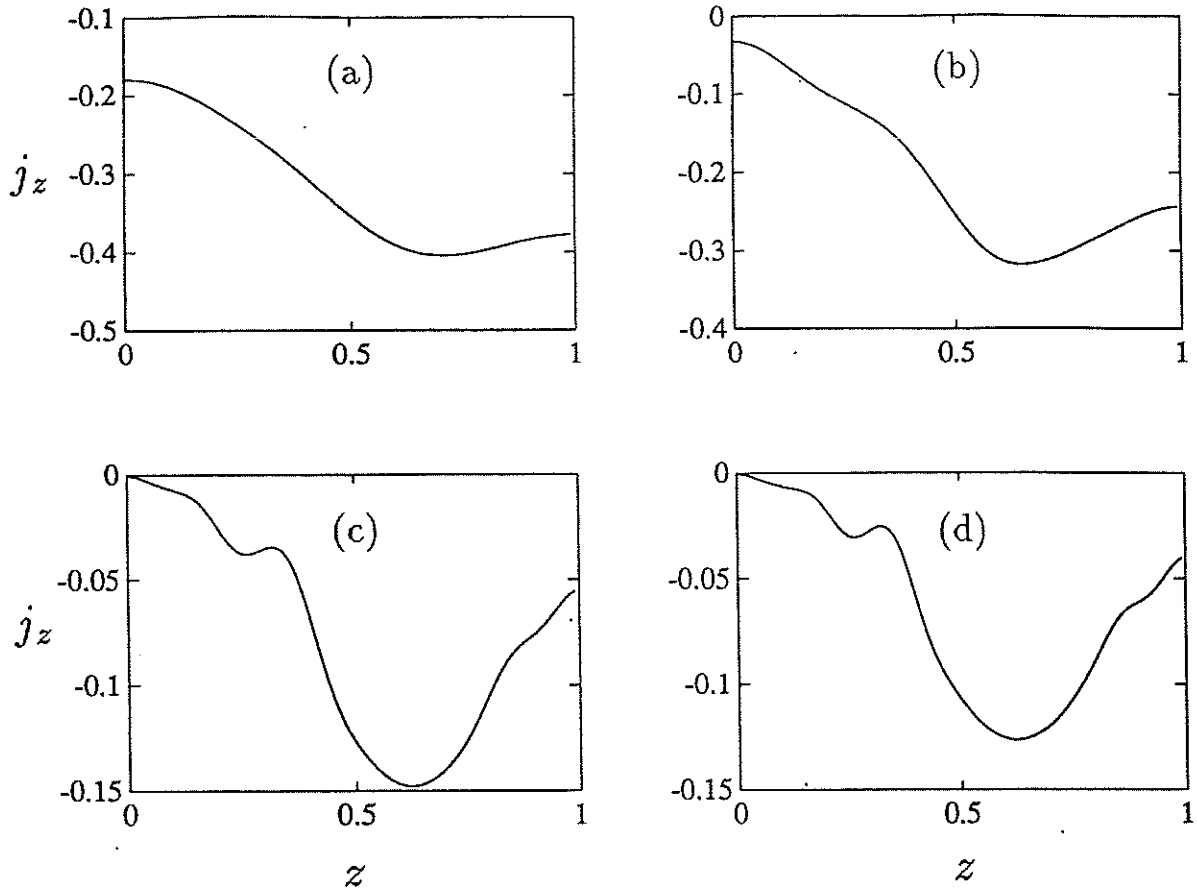

FIGURE 12. The evolution of j_z as Λ increases, for the cases shown in Figure 11.

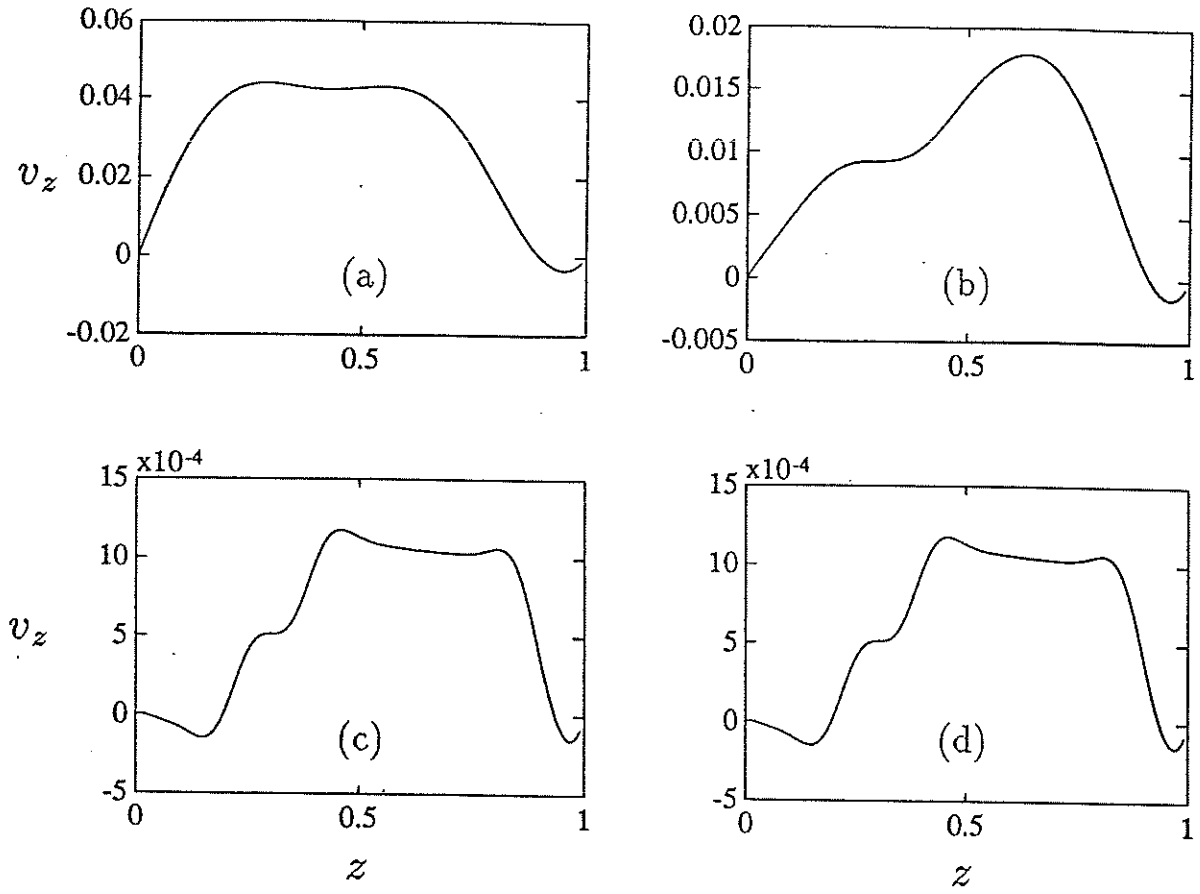

FIGURE 13. The evolution of v_z as Λ increases, for the cases shown in Figure 11.

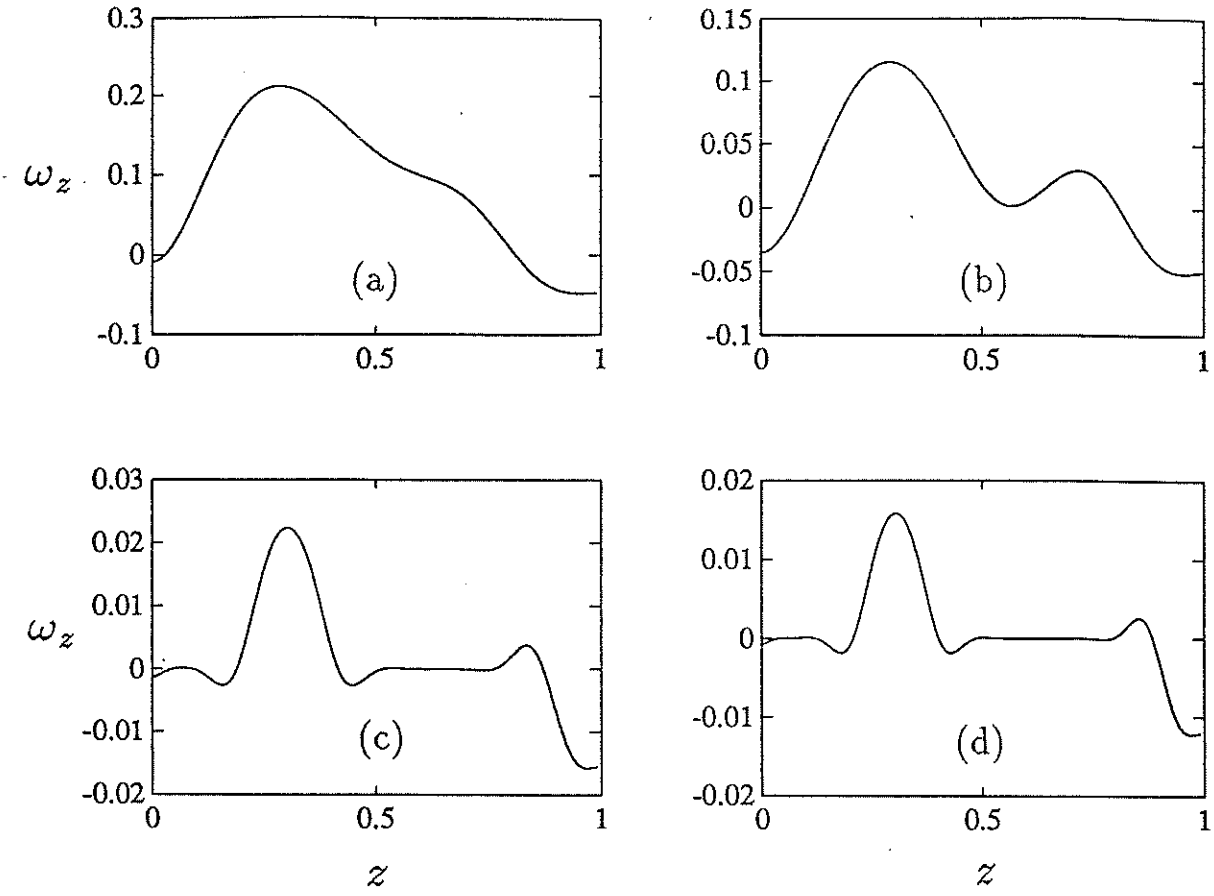

FIGURE 14. The evolution of ω_z as Λ increases, for the cases shown in Figure 11.

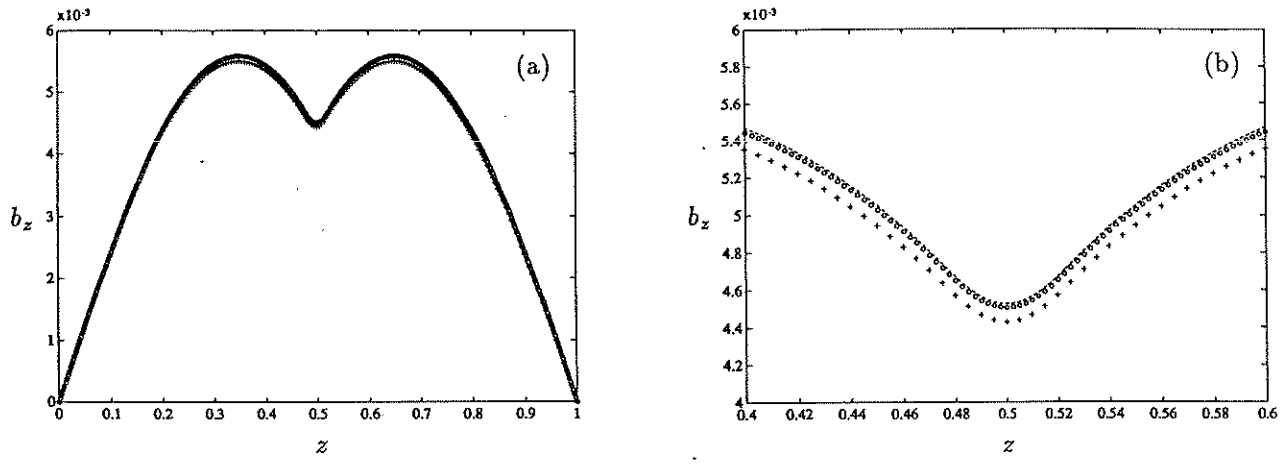

FIGURE 15. Convergence of b_z as the step size, h, is reduced; $\Lambda = 10^6$, $k_x = k_y = 1$, $q = \frac{3}{2}\pi$. Results for $h = 0.005, 0.0025$ and 0.00125 are marked by $+$, O and $-$, respectively. In (a) the full range $0 \leq z \leq 1$ is shown; in (b) only the vicinity of the critical point, $z_c = \frac{1}{2}$, is shown.

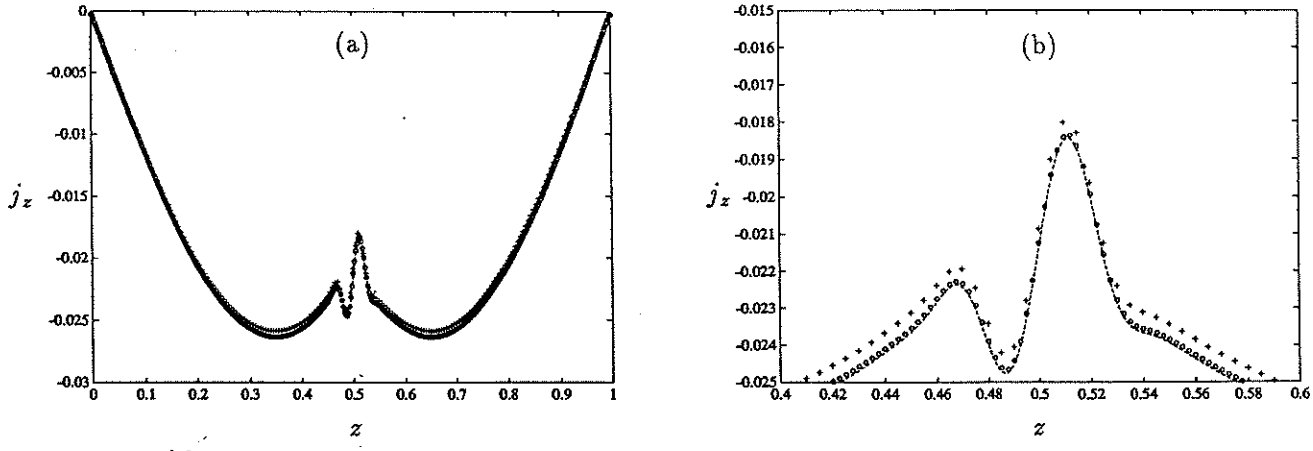

FIGURE 16. Convergence of j_z as the step size, h, is reduced; see caption to Figure 15.